Article

Cell Reports

Cancer-Cell-Intrinsic cGAS Expression Mediates Tumor Immunogenicity

Graphical Abstract

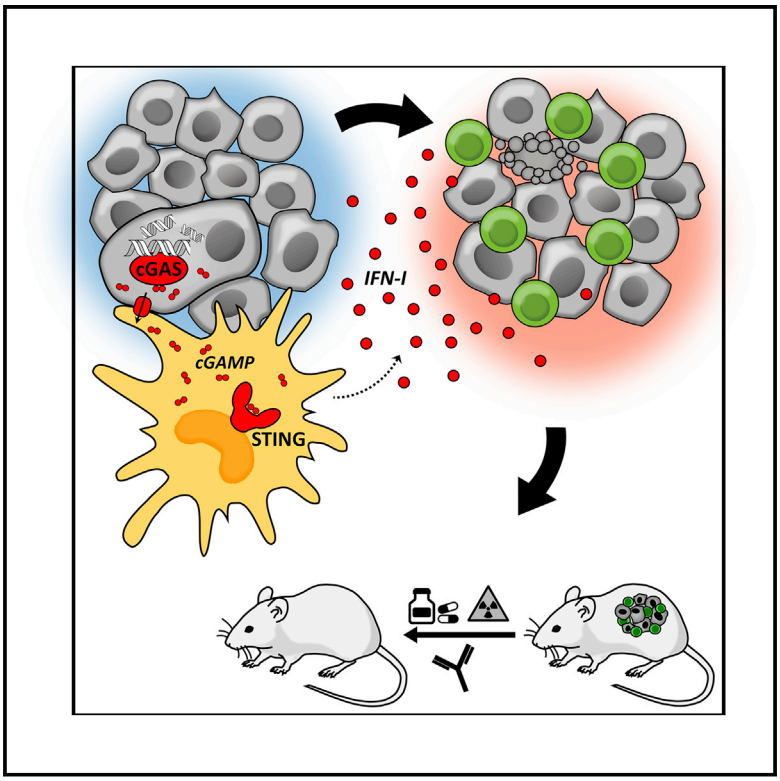

Highlights

- cGAS in cancer and STING in host cells are minimal requirements to activate $CD8^+$ T cells
- Cancer cells transfer cGAMP to myeloid cells in the TME that make STING-dependent IFN-I
- Cancer-cell-intrinsic cGAS improves tumor immunogenicity and response to therapy

Authors

Linda Schadt, Colin Sparano, Nicole Angelika Schweiger, ..., Zuzana Nascakova, Winfried Barchet, Maries van den Broek

Correspondence

vandenbroek@immunology.uzh.ch

In Brief

Schadt et al. show that cancer-cell-derived cGAMP is transferred to tumor-associated myeloid cells. Here, cGAMP activates STING and induces production of type I interferon. This promotes infiltration of protective $CD8^+$ T cells and improves survival as well as response to therapy.

Schadt et al., 2019, Cell Reports *29*, 1236–1248
October 29, 2019
https://doi.org/10.1016/j.celrep.2019.09.065

CellPress

OPEN ACCESS
CellPress

Cell Reports
Article

Cancer-Cell-Intrinsic cGAS Expression Mediates Tumor Immunogenicity

Linda Schadt,[1] Colin Sparano,[1] Nicole Angelika Schweiger,[1] Karina Silina,[1] Virginia Cecconi,[1] Giulia Lucchiari,[1] Hideo Yagita,[2] Emilien Guggisberg,[1] Sascha Saba,[1] Zuzana Nascakova,[3] Winfried Barchet,[4] and Maries van den Broek[1,5,*]

[1]Institute of Experimental Immunology, University of Zurich, Winterthurerstrasse 190, 8057 Zurich, Switzerland
[2]Department of Immunology, Juntendo University School of Medicine, Tokyo 113-8421, Japan
[3]Institute of Molecular Genetics of the ASCR, v. v. i., Videnska 1083, 142 20 Prague, Czech Republic
[4]Institute of Clinical Chemistry and Clinical Pharmacology, University Hospital and University of Bonn, Sigmund-Freud-Strasse 25, 35127 Bonn, Germany
[5]Lead Contact
*Correspondence: vandenbroek@immunology.uzh.ch
https://doi.org/10.1016/j.celrep.2019.09.065

SUMMARY

Sensing of cytoplasmic DNA by cyclic guanosine monophosphate-adenosine monophosphate (cGAMP) synthase (cGAS) results in production of the dinucleotide cGAMP and consecutive activation of stimulator of interferon genes (STING) followed by production of type I interferon (IFN). Although cancer cells contain supra-normal concentrations of cytoplasmic DNA, they rarely produce type I IFN spontaneously. This suggests that defects in the DNA-sensing pathway may serve as an immune escape mechanism. We find that cancer cells produce cGAMP that is transferred via gap junctions to tumor-associated dendritic cells (DCs) and macrophages, which respond by producing type I IFN *in situ*. Cancer-cell-intrinsic expression of cGAS, but not STING, promotes infiltration by effector CD8$^+$ T cells and consequently results in prolonged survival. Furthermore, cGAS-expressing cancers respond better to genotoxic treatments and immunotherapy. Thus, cancer-cell-derived cGAMP is crucial to protective anti-tumor CD8$^+$ T cell immunity. Consequently, cancer-cell-intrinsic expression of cGAS determines tumor immunogenicity and makes tumors hot. These findings are relevant for genotoxic and immune therapies for cancer.

INTRODUCTION

Cancer develops in the face of immune surveillance and thus needs to evade immune control to progress. The tumor microenvironment (TME) influences not only tumor progression but also the response to immune and standard therapies (Binnewies et al., 2018). Immunogenic or hot tumors contain more infiltrating T cells than cold tumors and are associated with favorable prognosis and better response to immune checkpoint inhibition (Galon et al., 2006; Van Allen et al., 2015). In contrast, cold tumors can be T cell excluded or T cell ignorant (Chen and Mellman, 2017; van der Woude et al., 2017), suggesting that multiple mechanisms may contribute to a tumor being cold. Besides the presence of infiltrating T cells, hot tumors are characterized by a type I interferon (IFN) signature (Gajewski et al., 2013). Indeed, type I IFN is essential for the generation of protective anti-tumor immunity, and tumor-infiltrating dendritic cells (DCs) are essential for both production of and response to type I IFN in the TME (Diamond et al., 2011; Fuertes et al., 2011; Dai et al., 2017; Dunn et al., 2006).

The production of type I IFN is downstream of the sensing of cytoplasmic double-stranded DNA (dsDNA) (Stetson and Medzhitov, 2006; Vanpouille-Box et al., 2018), which is normally absent from eukaryotic cells. However, substantial amounts of cytoplasmic dsDNA are found under pathological conditions, including viral infection, genomic instability, and DNA damage (Fenech et al., 2011; Harding et al., 2017; Ishikawa et al., 2009; Li and Chen, 2018; Mackenzie et al., 2017). Consistent with these findings, radiotherapy (Burnette et al., 2011; Deng et al., 2014) and chemotherapy (Ahn et al., 2014; Sistigu et al., 2014) induce type I IFN. Upon binding of dsDNA, cyclic guanosine monophosphate-adenosine monophosphate (cGAMP) synthase (cGAS) catalyzes the formation of the second messenger cGAMP. Subsequently, cGAMP binds to stimulator of interferon genes (STING), resulting in phosphorylation of interferon regulatory factor 3 (IRF3) and production of type I IFN (Ablasser et al., 2013a; Ishikawa and Barber, 2008; Li and Chen, 2018; Sun et al., 2013; Wu et al., 2013; Gao et al., 2013; recently reviewed in Ablasser and Chen, 2019).

Cancer cells often constitutively contain a high concentration of cytoplasmic dsDNA, which further increases upon DNA-damaging therapies such as radio- or chemotherapy (Shen et al., 2015). Given the important role of type I IFN in priming of protective T cell immunity (Diamond et al., 2011; Dunn et al., 2006; Fuertes et al., 2011), the presence of cytoplasmic dsDNA in cancer cells may contribute to their immunogenicity. Downregulation of the cGAS/STING pathway correlates with poor prognosis in human cancer (Song et al., 2017; Xia et al., 2016; Yang et al., 2017). Together, this suggests that the absence of cytoplasmic dsDNA sensing contributes to immune evasion of cancer cells.

It was proposed recently that cancer-cell-derived cytoplasmic dsDNA is transferred to tumor-associated DCs, resulting in cGAS/STING-dependent production of type I IFN by these DCs, priming of protective $CD8^+$ T cells, and tumor control (Woo et al., 2014). How cytoplasmic dsDNA is transferred from cancer cells to DCs, however, is largely unclear, although transfer via exosomes has been suggested (Kitai et al., 2017). In viral infections and carcinoma-astrocyte interactions, it was shown that cGAMP is transferred to neighboring cells via gap junctions, resulting in the activation of STING in cGAMP-receiving cells (Ablasser et al., 2013b; Chen et al., 2016).

Inspired by these observations, we proposed that cGAMP instead of cytoplasmic dsDNA is transferred from cancer cells to DCs, thus enabling the production of type I IFN and priming of protective immunity, even in situations where cancer cells have a compromised STING pathway. We show here that $CD8^+$ T-cell-mediated control of cancer depends on cancer-cell-derived cGAMP. This is in line with the recent observation that natural killer (NK)-cell-mediated control of tumor cells requires expression of STING by host cells and cGAS by cancer cells (Marcus et al., 2018), thus supporting our hypothesis. Furthermore, we show that cancer-cell-intrinsic cGAS makes tumors more sensitive to chemo-, radio-, and immunotherapy.

Thus, we propose that expression of cGAS by cancer cells determines tumor immunogenicity as well as its response to genotoxic and immune checkpoint inhibition therapies.

RESULTS

Production of Type I IFN in Co-cultures of DCs and Cancer Cells Requires Expression of cGAS by Cancer Cells and STING by DCs

To select an experimental system for testing whether cancer-cell-intrinsic cGAS expression contributes to tumor immunogenicity, we probed the cGAS/STING pathway in different murine tumor cell lines. Most cell lines expressed cGAS and/or STING, albeit different amounts (Figures 1A and S1A). To measure whether the cGAS/STING pathway is functional, we transfected the cell lines with DNA and quantified secreted type I IFN using a reporter cell line. All but two cell lines spontaneously produced very low amounts of type I IFN, which increased upon transfection with DNA (Figure 1B). In the CT26 cell line that is considered immunogenic, we next established CT26 mutants deficient for cGAS ($CT26^{\Delta Mb21d1}$) or STING ($CT26^{\Delta Tmem173}$) using CRISPR/Cas9 technology and validated the absence of cGAS or STING by western blot (Figure 1C). CT26 cells modified with an empty vector ($CT26^{ctrl}$) were used as control. In addition, we engineered cGAS-negative Lewis lung carcinoma (LLC; ATCC CRL-1642) cells (Figure 1A) to express cGAS (LLC^{Mb21d1}) and confirmed the expression of cGAS by western blot (Figure 1D).

As the STING pathway is frequently compromised in cancer cells (Song et al., 2017; Xia et al., 2016; Yang et al., 2017), they rely on other cell types for the production of immune-stimulating type I IFN. It has been suggested that tumor-associated DCs fulfill this role after uptake of cancer-cell-derived dsDNA (Klarquist et al., 2014; Woo et al., 2014). To study whether cancer cells can induce the production of type I IFN in DCs, we measured the amount of type I IFN in co-cultures (Figures 1E–1G and S1B–S1D). We observed a strong induction of type I IFN in co-cultures of $CT26^{ctrl}$ cells with wild-type bone-marrow-derived DCs (BMDCs) compared to cancer cells or BMDCs alone (Figures 1F and S1B). Type I IFN was absent from co-cultures of cGAS-deficient $CT26^{\Delta Mb21d1}$ cells with wild-type BMDCs (Figure 1F) but present in co-cultures of STING-deficient $CT26^{\Delta Tmem173}$ cells with BMDCs (Figure S1C). These data suggest that the production of type I IFN depends on cancer-cell-intrinsic expression of cGAS, but not STING. Co-cultures using cGAS-deficient BMDCs gave similar results to those using wild-type BMDCs, suggesting that expression of cGAS in BMDCs is dispensable for the production of type I IFN. Type I IFN was not detectable in co-cultures of any CT26 cell line with STING-deficient BMDCs (Figure 1F). This suggests that expression of STING in DCs is essential for the production type I IFN in co-cultures cGAS-expressing cancer cells. In line with the abovementioned findings, we observed that cGAS-overexpressing LLC^{Mb21d1} cells induce type I IFN secretion in co-cultured BMDCs, while the parental LLC cells do not (Figure 1G).

Intercellular transfer of cGAMP has been reported to depend on gap junctions (Ablasser et al., 2013b; Chen et al., 2016). To investigate whether cell-cell contact is indeed required for cGAMP transfer from cancer cells to DCs, we used a transwell system and found that the production of type I IFN was abrogated (Figure S1D). This excludes transfer of soluble or exosome-associated cGAMP.

To identify whether cGAMP is transferred from tumor cells to DCs over gap junctions, we generated connexin-43 (CX43)-deficient CT26 cells ($CT26^{\Delta Gja1}$) (Figure 1C). To assess the exchange of cytoplasm between cells, we used the calcein AM transfer assay (Figure S1E) (Ablasser et al., 2013b; Saccheri et al., 2010). $CT26^{\Delta Gja1}$ cells transferred significantly less calcein AM to co-cultured BMDCs than $CT26^{ctrl}$ cells (Figures S1F and S1G), suggesting that deleting *Gja1* is sufficient to reduce cytoplasmic exchange. We then co-cultured CX43-deficient $CT26^{\Delta Gja1}$ cells with BMDCs and found that the production of type IFN I was abolished (Figure 1F).

Thus, we showed that minimal requirements for production of type I IFN in cancer cell/BMDC co-cultures are the expression of cGAS in cancer cells and STING in BMDCs, suggesting transfer of cGAMP and not dsDNA from cancer cells to BMDCs. Furthermore, we showed that cGAMP is transferred via gap junctions *in vitro*.

Cancer-Cell-Intrinsic cGAS Deficiency Promotes Tumor Progression and Makes Tumors Cold

After having established that cancer-cell-intrinsic cGAS is essential for production of type I IFN by neighboring DCs *in vitro*, we investigated the contribution of cancer-cell-derived cGAMP on immune surveillance. Therefore, we injected $CT26^{ctrl}$, $CT26^{\Delta Mb21d1}$, or $CT26^{\Delta Tmem173}$ cells subcutaneously (s.c.) in BALB/c mice and monitored tumor growth and survival (Figure 2A). We found that cGAS-deficient, but not STING-deficient, CT26 tumors grow faster than control CT26 tumors (Figure 2B), resulting in significantly reduced survival (Figure 2C).

To exclude that the increased tumor growth of $CT26^{\Delta Mb21d1}$ cells is due to cell-intrinsic features, we measured the growth

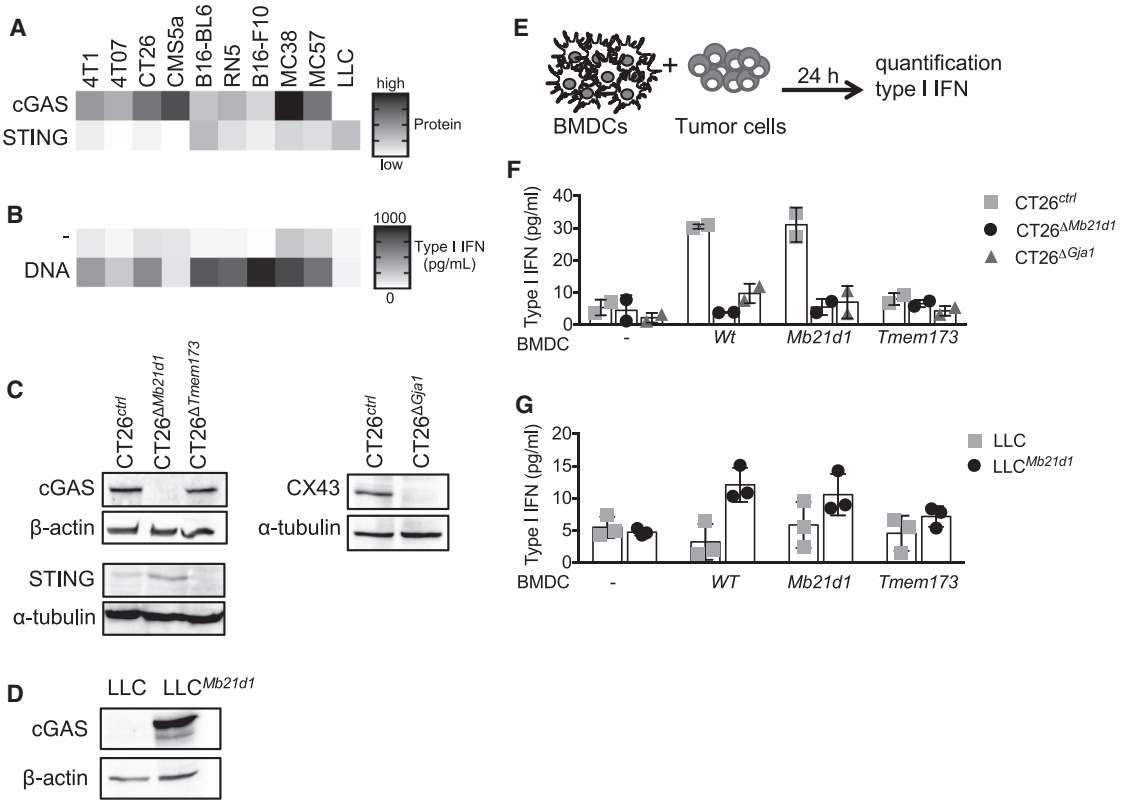

Figure 1. Production of Type I IFN in Co-cultures of DCs and Cancer Cells Requires Expression of cGAS by Cancer Cells and STING by DCs

(A) Expression of cGAS and STING protein in murine tumor cell lines *in vitro*. Expression was measured by western blot, and data are represented as relative protein expression in arbitrary units (cGAS/β-actin and STING/α-tubulin). The heatmap shows the range between low (white) to high (black) expression. Plots show pooled results from three independent experiments.

(B) *In vitro* production of type I IFN by murine tumor cell lines over 24 h. The upper row shows spontaneous production, and the lower row shows production of cells transfected with 1 μg genomic dsDNA. The heatmap shows the range between 0 pg/mL (white) and 1,000 pg/mL (black). Plots show pooled results from three independent experiments.

(C) Confirmation of deficiency of cGAS, STING, and connexin-43 (CX43) by western blot in CT26$^{\Delta Mb21d1}$, CT26$^{\Delta Tmem173}$, and CT26$^{\Delta Gja1}$ cells, respectively.

(D) Confirmation of cGAS overexpression in LLC^{Mb21d1} by western blot.

(E) Experimental design for (F) and (G). Cancer cells (0.15×10^6) were co-cultured with 0.5×10^6 bone marrow derived dendritic cells (BMDCs) from wild-type (WT), cGAS-deficient (*Mb21d1*) or STING-deficient (*Tmem173*) mice. After 24 h, type I IFN was measured in the supernatant with the reporter cell line LL171. Every symbol represents one biological replicate. Bars represent mean ± SD. Results are representative of 2 independent experiments each.

(F) CT26^{ctrl}, CT26$^{\Delta Mb21d1}$, and CT26$^{\Delta Gja1}$ cancer cells.

(G) LLC and LLC^{Mb21d1} cancer cells.

See also Figure S1.

of CT26^{ctrl}, CT26$^{\Delta Mb21d1}$, or CT26$^{\Delta Tmem173}$ cancer cells *in vitro* and found no significant difference (Figure S2A). Next, we injected CT26^{ctrl}, CT26$^{\Delta Mb21d1}$, or CT26$^{\Delta Tmem173}$ cells in NOD.Cg-*Prkdc*^{scid} *Il2rg*^{tm1Wjl} (NSG) mice that lack T, B, and NK cells (Figure S2B). All three CT26 cell lines showed similar growth and survival characteristics (Figures S2C and S2D), suggesting that the increased growth of cGAS-deficient CT26 tumors is due to compromised immune surveillance.

To further support the role of cancer-cell-derived cGAMP in immune control of tumors, we analyzed the immune infiltrates associated with CT26^{ctrl}, CT26$^{\Delta Mb21d1}$, and CT26$^{\Delta Tmem173}$ tumors in BALB/c mice 22 d after tumor cell injection (Figure 2D). Within the CD45$^+$ leukocyte population, the proportions of CD3$^+$, CD8$^+$, and CD8$^+$ IFN-γ$^+$ T cells were significantly lower in cGAS-deficient tumors than control or STING-deficient tumors (Figures 2E and S2E). To address whether the tumor-specific CD8$^+$ T cell population is influenced by the absence of cGAS in cancer cells, we analyzed IFN-γ production by tumor-associated CD8$^+$ T cells after *in vitro* stimulation with a cancer-cell-specific peptide, AH-1 (Huang et al., 1996) (Figure 2F, left panel, and Figure S2F). In addition, we saw that cGAS-expressing tumors contained a higher proportion of CD39$^+$ cells within the CD8$^+$ population (Figure 2F, right panel, and Figure S2F), suggesting an increase in tumor-specific CD8$^+$ T cells (Simoni et al., 2018). Our observation that cGAS-proficient tumors contain higher concentrations of the T-cell-derived effector cytokines IFN-γ and tumor necrosis factor alpha (TNF-α) further substantiates that cGAS-expressing tumors are hot (Figure 2G). The proportion of other immune cells like CD4$^+$ and FoxP3$^+$ CD4$^+$ T cells as well as myeloid cells were comparable in the different tumors

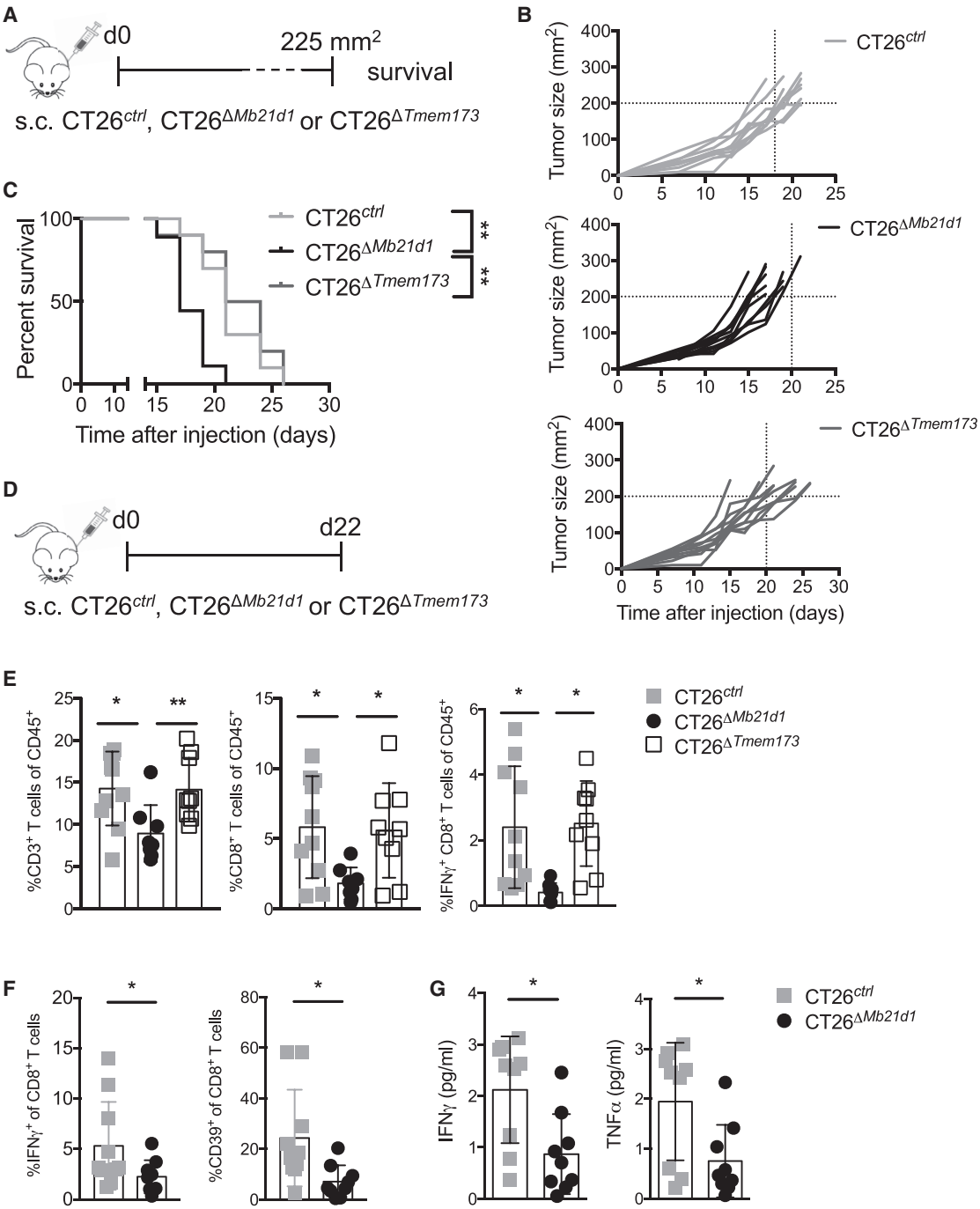

Figure 2. Cancer-Cell-Intrinsic cGAS Expression Makes Tumors Hot and Promotes Immune Surveillance

(A) Experimental design for (B) and (C). CT26^{ctrl}, CT26$^{\Delta Mb21d1}$, or CT26$^{\Delta Tmem173}$ cells were injected subcutaneously into BALB/c mice (n = 10 mice per group).

(B) Tumor size was measured with a caliper. Every line represents an individual mouse. Results are representative of four independent experiments.

(C) Survival curve. Death event is defined as tumor size >225 mm^2. Statistics were calculated using the log-rank (Mantel-Cox) test. Results are representative of four independent experiments. **$p < 0.01$.

(D) Experimental design for (E)–(G). CT26^{ctrl}, CT26$^{\Delta Mb21d1}$, or CT26$^{\Delta Tmem173}$ cells were injected subcutaneously into BALB/c mice (n = 9–10 mice per group).

(E) Percentage of immune cells in tumors analyzed by flow cytometry at the endpoint (day 22). Percentage of IFN-γ^+ CD8$^+$ T cells in tumors was determined after *in vitro* stimulation with phorbol 12-myristate 13-acetate (PMA)/ionomycin in the presence of brefeldin A. Every symbol represents an individual mouse. Bars represent mean ± SD. Statistics were calculated using one-way ANOVA with Tukey's multiple comparison correction. Gating strategies are shown in Figure S2E. Results are representative of three independent experiments.

(legend continued on next page)

(Figure S2G; data not shown). Moreover, we found no differences in the proportion of NK cells in the different tumors (Figure S2H). For gating strategies, see Figures S2I and S2J, respectively.

Depletion of $CD8^+$ T cells promoted the growth of $CT26^{ctrl}$, but not $CT26^{\Delta Mb21d1}$, tumors (Figure S2K). This underscores the relevance of $CD8^+$ T cells for controlling CT26 tumor growth as well as the importance of cancer-cell-intrinsic cGAS for recruiting those T cells (Figure 2E).

To substantiate our findings, we monitored tumor growth and survival of C57BL/6 mice that were injected with LLC or LLC^{Mb21d1} cells (Figure S3A). We found that the overexpression of cGAS in LLC cells resulted in slower tumor growth (Figure S3B), prolonged survival (Figure S3C), and an infiltrate reminiscent of hot tumors (Figures S3D and S3E**)**. To strengthen the concept that type I production in the TME depends on the transfer of cGAMP, but not DNA, from cancer to host cells, we injected LLC or LLC^{Mb21d1} in wild-type C57BL/6 or cGAS-deficient B6(C)-*Cgas*$^{tm1d(EUCOMM)Hmgu}$/J ($cGAS^{-/-}$ B6) mice (Figure S3F). As shown above, LLC^{Mb21d1} tumors contained more effector $CD8^+$ T cells than LLC tumors, independently of the mouse genotype (Figures S3G and S3H). These data suggest that the DNA-sensing capacity of the host is insignificant for the generation of antitumor immunity.

Thus, cancer-cell-intrinsic cGAS expression promotes infiltration by effector $CD8^+$ T cells that control tumor growth.

Cancer-Cell-Derived cGAMP Induces Production of Type I IFN by Tumor-Associated DCs

Using co-cultures of cancer cells and BMDCs, we showed that cancer-cell-derived cGAMP is transferred to DCs, which produce type I IFN in turn. To investigate whether this process is operative in tumors *in vivo*, we isolated established $CT26^{ctrl}$ and $CT26^{\Delta Mb21d1}$ tumors from BALB/c mice (Figure 3A). From half of the tumors, we prepared a lysate; the other half was processed for single-cell analysis by flow cytometry. The lysate of cGAS-deficient CT26 tumors contained significantly less IFN-β than that of control CT26 tumors (Figure 3B). To identify the cell type that produces type I IFN in CT26 tumors, which we consider a proxy for uptake of cancer-cell-derived cGAMP, we used PrimeFlow. We applied this flow-cytometry-based method to detect transcripts in single cells, because intracellular staining for type I IFN using antibodies is not sufficiently sensitive or reliable (Lienenklaus et al., 2009; Scheu et al., 2008). We stained $CT26^{ctrl}$ and $CT26^{\Delta Mb21d1}$ tumors for different lineage markers as well as *Ifnb1* transcripts. We detected the *Ifnb1* signal almost exclusively in the $CD45^+$ leukocyte fraction (Figure 3C). We found a significantly higher percentage of $Ifnb1^+$ cells within the leukocyte fraction of $CT26^{ctrl}$ tumors than in cGAS-deficient $CT26^{\Delta Mb21d1}$ tumors (Figure 3D). Moreover, the majority of $Ifnb1^+$ cells in $CT26^{ctrl}$ tumors were DCs and macrophages, of which both were reduced in cGAS-deficient $CT26^{\Delta Mb21d1}$ tumors (Figures 3E and S4A). Conventional DC1s (cDC1s) and cDC2s differ concerning their capacity to activate T cells and can be discriminated by surface expression of CD11b or CD103 (Broz et al., 2014). We saw that both cDC1s and cDC2s expressed significantly higher amounts of *Ifnb1* transcripts in $CT26^{ctrl}$ tumors than in cGAS-deficient $CT26^{\Delta Mb21d1}$ tumors (Figures S4B and S4C). Comparison of the *Ifnb1* signal in tumor-associated, major histocompatibility complex class II $(MHCII)^+$ cells to that in $MHCII^+$ naive spleen cells (negative control) or $MHCII^+$ spleen cells stimulated *in vitro* with a STING agonist (positive control) technically validated this readout (Figure S4D).

Thus, DCs and macrophages associated with cGAS-expressing tumors produce type I IFN *in situ*, whereas their ability to do so is compromised in cGAS-deficient tumors. This suggests that cancer-cell-derived cGAMP indeed is transferred to neighboring myeloid cells.

The Efficacy of DNA-Damaging Cancer Therapies Depends on Cancer-Cell-Intrinsic Expression of cGAS

In response to DNA damage, genomic instability, or viral infection, the amount of cytoplasmic dsDNA is increased in eukaryotic cells (Fenech et al., 2011; Harding et al., 2017; Ishikawa et al., 2009; Mackenzie et al., 2017). Since cytoplasmic dsDNA is the substrate for cGAS, we investigated the effect of genotoxic treatments on immune-mediated control of cGAS-deficient and control CT26 tumors. First, we confirmed that the amount of cytoplasmic dsDNA in untreated CT26 cancer cells is indeed higher compared to untransformed cells by ~100-fold (Figure S5A). We then applied genotoxic stress to CT26 cells *in vitro* to validate an increase of the cytoplasmic dsDNA concentration. Different genotoxic treatments including radiation with 8 Gy or 20 Gy as well as exposure to 15 μM cisplatin increased the amount of cytoplasmic DNA significantly (Figure S5A).

Second, we investigated whether cGAS-deficient cancer cells have a decreased sensitivity to genotoxic treatments per se and determined the survival of $CT26^{ctrl}$ or $CT26^{\Delta Mb21d1}$ cancer cells after treatment with radiation or cisplatin (Figure S5B). We found that both cell lines showed a similar decrease in the surviving fraction upon increasing doses of radiotherapy and cisplatin (Figure S5B). In addition, we observed similar radiation-induced DNA damage in $CT26^{ctrl}$ or $CT26^{\Delta Mb21d1}$ cells as measured by gamma-H2AX staining (Figure S5C and S5D). This suggests that the sensitivity toward genotoxic treatments is not influenced by the absence of cGAS in CT26 cancer cells.

Third, we analyzed the immune-stimulating effect of radiotherapy in mice bearing cGAS-deficient or control CT26 tumors. Therefore, we subjected BALB/c mice bearing established

(F) Percentage of IFN-γ^+ (left panel) and $CD39^+$ (right panel) cells within the $CD8^+$ T cell population in the tumor analyzed by flow cytometry at the endpoint (day 17) after *in vitro* stimulation with AH-1 peptide in the presence of brefeldin A. Every symbol represents an individual mouse. Bars represent mean ± SD. Statistics were calculated using the Mann-Whitney *U* test. Gating strategies are shown in Figure S2F. Results are representative of two independent experiments.
(G) Concentration of IFN-γ and TNF-α in tumor lysate normalized to total protein concentration measured at the endpoint (day 22). Every symbol represents an individual mouse. Bars represent mean ± SD. Statistics were calculated using unpaired two-tailed Student's t test. *$p < 0.05$, **$p < 0.01$. Results are representative of two independent experiments.
See also Figures S2 and S3.

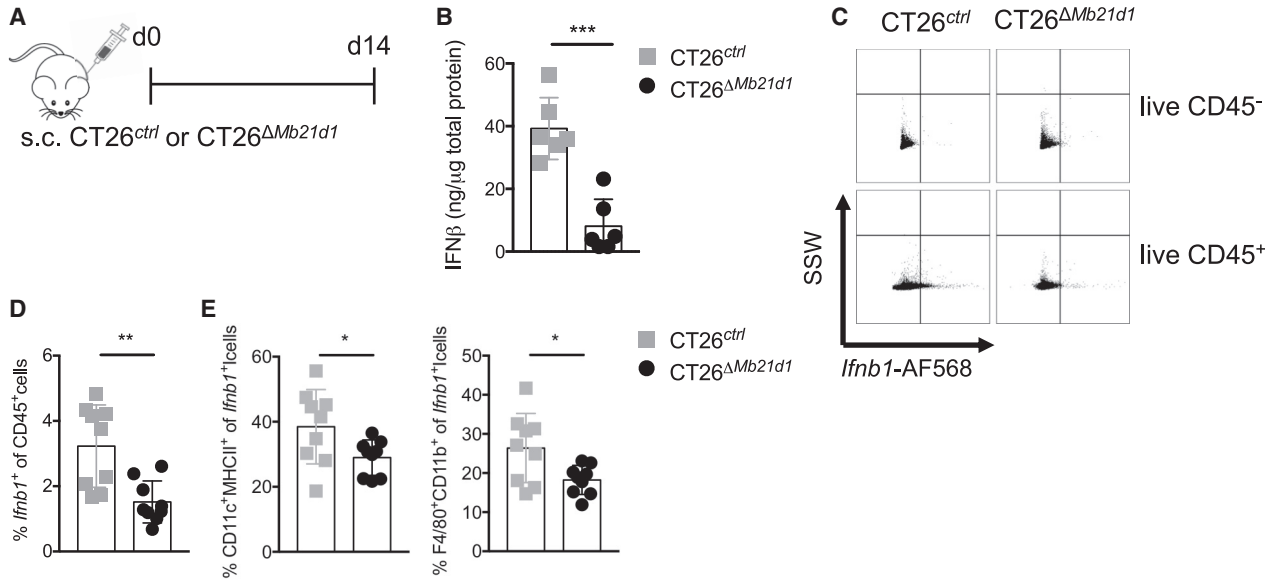

Figure 3. Cancer-Cell-Derived cGAMP Induces the Production of IFN-β by Tumor-Associated DCs

(A) Experimental design. CT26^{ctrl} or CT26$^{\Delta Mb21d1}$ cells were injected subcutaneously into BALB/c mice (n = 10 mice per group).

(B) IFN-β concentration in tumor lysate normalized to total protein concentration measured at the endpoint (day 14). Every symbol represents an individual mouse.

(C) Representative plots for measurement of *Ifnb1* mRNA by flow cytometry in CT26^{ctrl} and CT26$^{\Delta Mb21d1}$ tumors. The upper panels are gated on live, CD45$^-$ cells. The lower panels are gated on live, single CD45$^+$ cells.

(D) Percentage of *Ifnb1*$^+$ cells in the CD45$^+$ population at the endpoint (d 14).

(E) Percentage of DCs and macrophages of all live, single *Ifnb1*$^+$ cells. DCs were gated as CD45$^+$CD11c$^+$MHCII$^+$ and macrophages as CD45$^+$CD11b$^+$F4/80$^+$ cells.

Every symbol represents an individual mouse. Bars represent mean ± SD. Statistics were calculated using unpaired two-tailed Student's t test. *p < 0.05, **p < 0.01, ***p < 0.005. Gating strategies are shown in Figure S4A. Results are representative of two independent experiments.

See also Figure S4.

CT26^{ctrl} or CT26$^{\Delta Mb21d1}$ tumors to radiotherapy given as a single dose of 20 Gy (Surace et al., 2015) (Figure 4A). As shown above, untreated CT26$^{\Delta Mb21d1}$ tumors grew faster than untreated CT26^{ctrl} tumors (Figure 4B), which resulted in a shorter survival (Figure 4C). Although both tumors responded to radiotherapy, therapy-induced growth retardation and increase in survival was only marginal in mice bearing cGAS-deficient tumors. In contrast, the clinical response of mice bearing CT26^{ctrl} tumors was very pronounced and resulted in tumor clearance in 3 out of 10 mice (Figures 4B and 4C). Radiotherapy supports CD8$^+$ T-cell-mediated immunity (Gupta et al., 2012; Surace et al., 2015; Galluzzi et al., 2017); therefore, we characterized immune infiltrates in irradiated and untreated tumors. We found that numbers of CD3$^+$ and CD8$^+$ T cells were increased upon radiotherapy in CT26^{ctrl} tumors, but not cGAS-deficient CT26$^{\Delta Mb21d1}$ tumors (Figure S5E).

We used a similar experimental setup to compare the sensitivity of CT26^{ctrl} or CT26$^{\Delta Mb21d1}$ tumors to another genotoxic treatment, cisplatin (Figure 4D). Cisplatin significantly retarded tumor growth and prolonged survival of mice bearing CT26^{ctrl} tumors (Figures 4E and 4F). In contrast, cisplatin had no effect on the growth of cGAS-deficient CT26$^{\Delta Mb21d1}$ tumors (Figure 4E), nor did it increase survival (Figure 4F).

Thus, although radiotherapy and cisplatin have a different mode of action, both induce higher concentrations of cytoplasmic dsDNA. This explains why both genotoxic therapies show only limited or even no clinical efficacy when tumors lack the expression of cGAS and consequently cannot process the dsDNA into immune-stimulating cGAMP.

cGAS-Expressing Tumors Respond Better to Immune Checkpoint Inhibition

Several reports described that hot tumors respond better to immune checkpoint inhibition (Ayers et al., 2017; Van Allen et al., 2015). Since cGAS-expressing tumors have a hot phenotype, we hypothesized that treatment with anti-PD1 plus anti-CTLA4 is more efficacious in such tumors. To test this, we treated mice bearing CT26^{ctrl} or CT26$^{\Delta Mb21d1}$ tumors with anti-PD1 plus anti-CTLA monoclonal antibodies and monitored tumor growth and survival (Figure 5A). As shown in Figures 2 and 4, untreated CT26$^{\Delta Mb21d1}$ tumors grew faster than untreated CT26^{ctrl} tumors, which resulted in a shorter survival (Figures 5B and 5D). Although both tumors responded to the checkpoint inhibitor treatment, CT26^{ctrl} tumors responded significantly better than cGAS-deficient CT26$^{\Delta Mb21d1}$ concerning the survival of these mice (Figure 5D). We observed complete tumor rejection in 8 out of 20 mice with CT26^{ctrl} tumors but only 2 out of 20 mice with CT26$^{\Delta Mb21d1}$ tumors (Figure 5C).

Cancer-Cell-Intrinsic Expression of cGAS Correlates with Infiltration of CD8$^+$ T Cells in Human Microsatellite-Stable Colorectal Cancer

To determine the clinical relevance of our findings, we analyzed colorectal adenocarcinoma resection specimens from 25

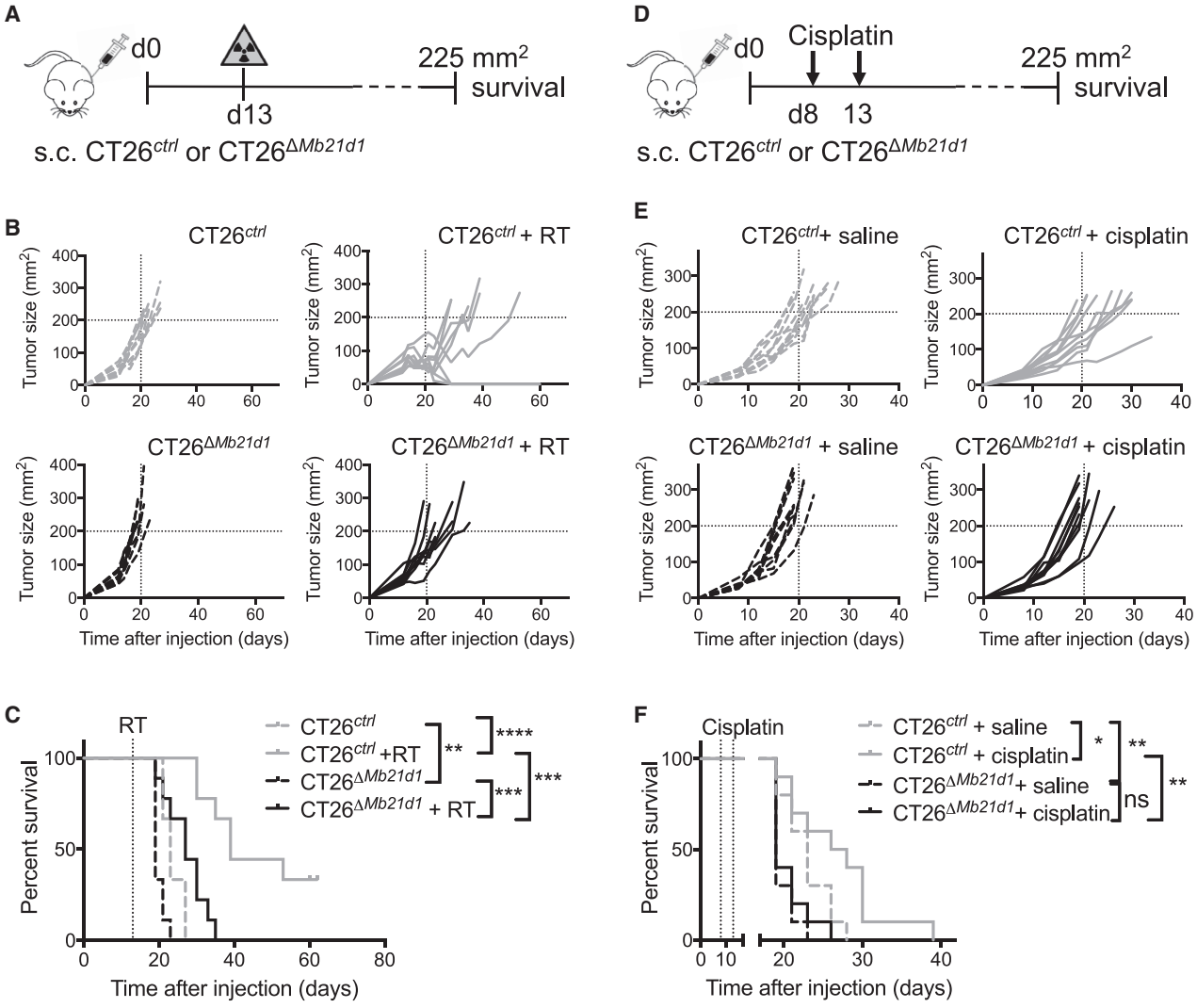

Figure 4. The Efficacy of DNA-Damaging Cancer Therapies Depends on Cancer-Cell-Intrinsic Expression of cGAS

(A) Experimental design for (B) and (C). CT26^{ctrl} or CT26$^{\Delta Mb21d1}$ cells were injected subcutaneously into BALB/c mice (n = 10 mice per group). Radiotherapy (RT; 1× 20 Gy) was applied to the tumor on day 13.

(B) Tumor size was measured with a caliper. Every line represents an individual mouse.

(C) Survival curve. Death event is defined as tumor size >225 mm^2. Statistics were calculated using the log-rank (Mantel-Cox) test. **p < 0.01, ***p < 0.005, ****p < 0.001.

(D) Experimental design for (E) and (F). CT26^{ctrl} or CT26$^{\Delta Mb21d1}$ cells were injected subcutaneously into BALB/c mice (n = 10 mice per group). Mice were treated with cisplatin (3 mg/kg) or saline on days 8 and 13.

(E) Tumor size was measured with a caliper. Every line represents an individual mouse.

(F) Survival curve. Death event is defined as tumor size >225 mm^2. Statistics were calculated using the log-rank (Mantel-Cox) test. *p < 0.05, **p < 0.01.

See also Figure S5.

patients. Using four-color multiplex immunofluorescence, we stained for cGAS, pan-cytokeratin (PanCK; epithelial cells), and CD8 (CD8$^+$ T cells) (Figure 6A). Our abovementioned data suggest that cancer-cell-intrinsic expression of cGAS characterizes hot tumors. Therefore, we specifically analyzed cGAS expression by tumor cells. We first applied an algorithm to segment the tissue in tumor and stroma based on expression of PanCK and morphology (Figure 6B). We then determined which proportion of cancer cells expressed cGAS (Figure 6C) and quantified the number of CD8$^+$ T cells per image (Figure 6D). We found that only 15 out of 151 tumor images contained >10% cGAS$^+$ cancer cells (Figure 6E), whereas cGAS expression was detectable in all patients in the tumor-adjacent non-diseased tissue (Figure S6). We found a significant correlation between the percentage of cancer cells that express cGAS and the density of tumor-infiltrating CD8$^+$ T cells (Figure 6E). In one patient with heterogeneous expression of cancer-cell-intrinsic cGAS, we saw that CD8$^+$ T cells were mainly present in areas with cGAS expression (Figure 6F). This underscores the concept that cancer-cell-intrinsic cGAS directly drives the infiltration of CD8$^+$ T cells.

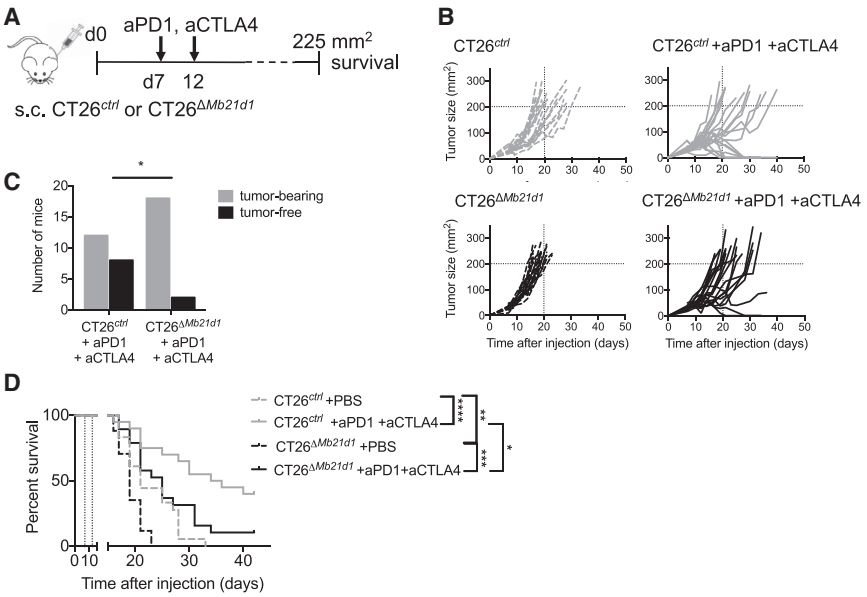

Figure 5. cGAS-Expressing Tumors Respond Better to Immune Checkpoint Inhibition

(A) Experimental design for (B)–(D). $CT26^{ctrl}$ or $CT26^{\Delta Mb21d1}$ cells were injected subcutaneously into BALB/c mice (n = 10 mice per group). On days 7 and 12, mice were injected intraperitoneally (i.p.) with 250 μg anti-PD1 (RMP1-14) and 250 μg anti-CTLA4 (9H10) antibodies or PBS.

(B–D) Pooled data from two identical experiments. (B) Tumor size was measured with a caliper. Every line represents an individual mouse. (C) Number of tumor-bearing and tumor-free mice in $CT26^{ctrl}$ or $CT26^{\Delta Mb21d1}$ after treatment with anti-PD1 and anti-CTLA4. Bars represent the total number of mice per group. Statistics were calculated using the chi-square test. (D) Survival curve. Death event is defined as tumor size >225 mm^2. Statistics were calculated using the log-rank (Mantel-Cox) test. *p < 0.05, **p < 0.01, ***p < 0.005, ****p < 0.001.

Thus, also in humans, cancer-cell-intrinsic cGAS expression positively correlates with T cell infiltration.

DISCUSSION

In this study, we have shown that cGAS expression in cancer cells is critical for tumor control by $CD8^+$ T cells. Cancer cells have plenty of substrate for cGAS because of their unusually high concentration of cytoplasmic dsDNA (Li and Chen, 2018). Consequently, cancer cells can produce substantial amounts of cGAMP. We uncovered that *in vitro* cGAMP is transferred via gap junctions from cancer cells to DCs, where it induces the production of type I IFN in a STING-dependent fashion. This is in line with the observations that intra-tumoral or even systemic application of STING agonists (Corrales et al., 2015; Dai et al., 2017; Li et al., 2016; Ramanjulu et al., 2018) or induction of gap junctions between cancer cells and DCs (Saccheri et al., 2010) improves immune surveillance. Furthermore, we found that cancer-cell-intrinsic cGAS is critical for the efficacy of genotoxic treatments such as radio-, chemo-, and immunotherapy.

Although initially known for antiviral activity, type I IFN influences immunity via direct action on innate and adaptive lymphocytes. For example, type I IFN activates NK cells to execute potent antiviral (Biron et al., 1999) and anti-tumor defense (Swann et al., 2007). In addition, type I IFN is essential for rejection of tumors by $CD8^+$ T cells (Diamond et al., 2011; Dunn et al., 2006; Fuertes et al., 2011). The connection between type I IFN and the cGAS/STING pathway has been appreciated for some time (Stetson and Medzhitov, 2006), and the importance of this pathway for control of cancer has recently received increasing attention (reviewed in Vanpouille-Box et al., 2018). According to the current view, cancer-cell-derived DNA obtains access to the cytoplasm of host cells via an unknown mechanism (Woo et al., 2014) or exosomes (Kitai et al., 2017), resulting in STING-dependent production of type I IFN by the latter. This view is challenged by our results and work recently reported by Marcus et al. (2018) showing that cGAMP, and not dsDNA, is transferred from cancer cells to DCs.

The pivotal role of STING-dependent production of type I IFN by tumor-infiltrating myeloid cells (DCs and macrophages) concerning the generation of protective anti-tumor immunity was shown in several studies (Corrales et al., 2015; Marcus et al., 2018; Woo et al., 2014). However, which upstream events induce STING signaling in tumor-infiltrating DCs was not completely understood. We identified cancer-cell-derived cGAMP as the molecule that induces STING-dependent type I IFN production by DCs and macrophages, suggesting that host cGAS is dispensable for this response. Indeed, it has been shown in different tumor models that cGAS deficiency in the host does not influence tumor growth (Marcus et al., 2018; Wang et al., 2017). Along these lines, our *in vivo* data show that the immune infiltration of tumors from wild-type and cGAS-deficient mice is comparable for both hot and cold tumors. Additionally, we confirmed *in vitro* that the production of type I IFNs required cGAS expression in cancer cells and STING expression in DCs. Our data, together with previously published work, indicate that cGAMP, and not dsDNA, induces STING-activation in myeloid cells, including DCs and macrophages, and the consequent activation of the adaptive immune system. How cGAMP is transferred *in vivo* from cancer to immune cells has not been determined yet.

We showed that cancer-cell-intrinsic expression of cGAS and consequent production of cGAMP promotes tumor control by $CD8^+$ T cells, mainly by driving their differentiation into effectors. The same mechanism accounts for control of tumors that are recognized by NK cells rather than $CD8^+$ T cells (Marcus et al., 2018). Both studies together make a strong cause for the importance of cancer-cell-intrinsic expression of cGAS in the defense against cancer by innate as well as adaptive immune cells. Being equally important for innate and adaptive

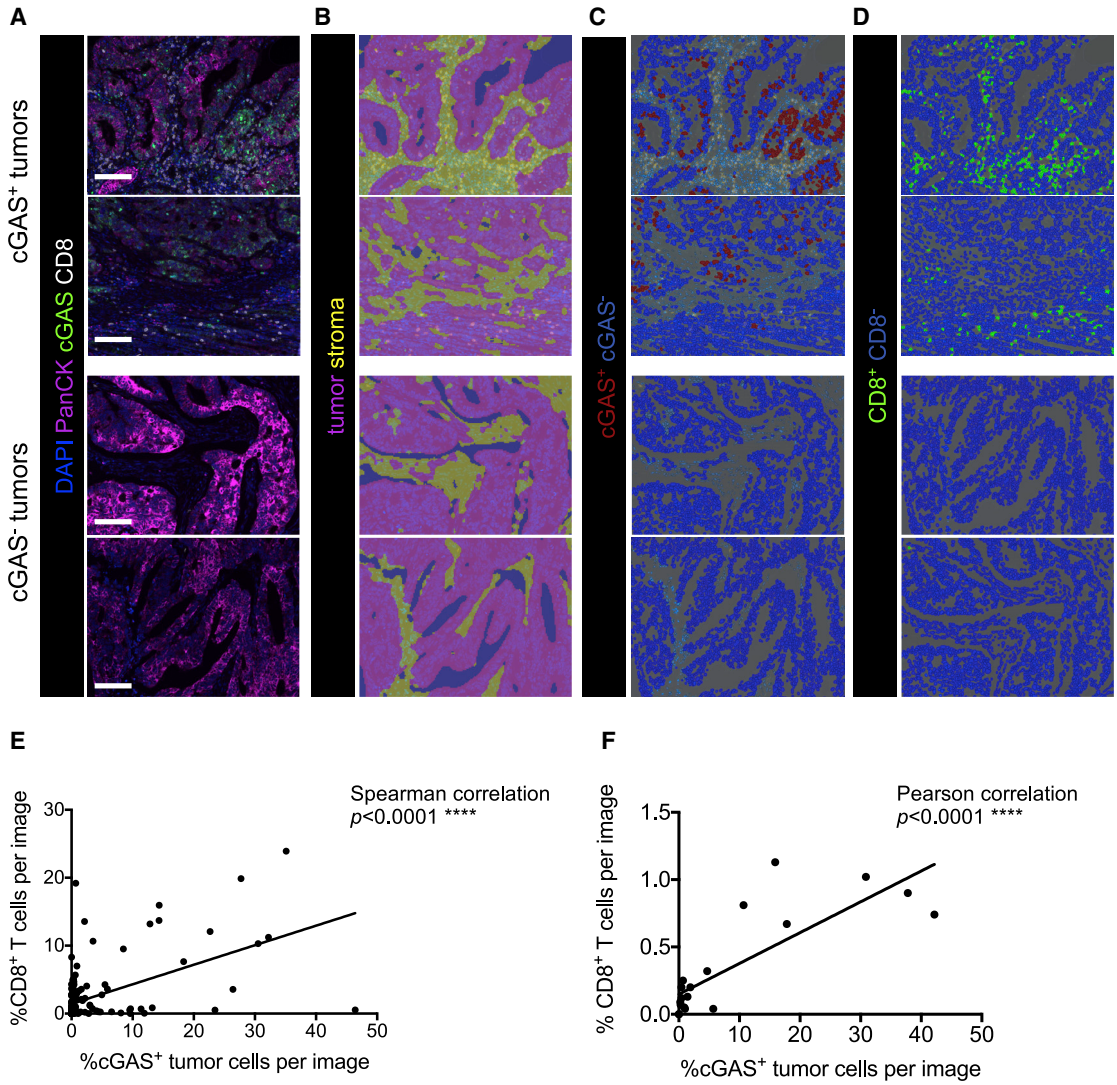

Figure 6. Cancer-Cell-Intrinsic Expression of cGAS Correlates with Infiltration of CD8$^+$ T Cells in Human Microsatellite-Stable Colorectal Cancer

(A) Representative images of four-color multiplex immunofluorescence on resection specimens from four colorectal adenocarcinoma patients. Staining shows cGAS (green), epithelial cells (PanCK, magenta), CD8$^+$ T cells (CD8, white), and nuclear staining (DAPI, blue). Scale bar represents 100 μm.

(B) Representative images of the applied tissue segmentation algorithm to differentiate tumor (magenta) and stroma (yellow) based on morphology and PanCK expression.

(C) Representative images of the applied cell segmentation and scoring algorithm in the tumor area for cGAS-positive (red), and -negative (blue).

(D) Representative images of the applied cell segmentation and scoring algorithm in the tumor and stroma for CD8-positive (green) and -negative (blue) cells.

(E) Correlation of the percentage of cGAS$^+$ tumor cells and the percentage of CD8$^+$ T cells per image. Every symbol represents one image; in total, 151 images were analyzed from 25 patients. At least 6 images were analyzed per patient. Statistics were calculated using nonparametric Spearman correlation.

(F) Correlation of the percentage of cGAS$^+$ tumor cells and the percentage of CD8$^+$ T cells in one patient with a heterogeneous distribution of cGAS expression in the tumor. Every symbol represents one image; in total, 20 images were analyzed from patient 14. Correlation was calculated using a parametric Pearson test. Statistics were calculated using the Pearson correlation coefficient.

See also Figure S6.

immunity against cancer assigns a key role to cGAS among immune regulators.

We showed that cancer-cell-intrinsic expression of cGAS influences the quality of immune infiltration in human colorectal adenocarcinoma. Since CD8$^+$ T cell infiltration correlates with increased survival of cancer patients in many disease entities, analysis of cGAS expression by cancer cells may be a potential biomarker for survival or response to (immune) therapies. We observed that tumor-adjacent non-diseased tissues in all patients expressed cGAS in epithelial and stromal cells, whereas cGAS expression was rare in carcinoma cells. This suggests that loss of cGAS is

an immune escape mechanism and goes in line with the observation that the loss of cGAS expression correlates with progression of colorectal cancer (Xia et al., 2016; Yang et al., 2017).

Although most cancer cells contain a substantial concentration of cytoplasmic dsDNA, this can further be increased by genotoxic stress (Harding et al., 2017; Härtlova et al., 2015; Sheng et al., 2018). This explains why immune stimulation by genotoxic treatment is cGAS/STING dependent and radiotherapy is less efficient in STING-deficient mice (Deng et al., 2014). Also, combining radiotherapy with a STING agonist improved therapeutic efficacy (Baird et al., 2016). Moreover, artificially enhancing the concentration of cytoplasmic DNA and cyclic dinucleotides in dying cancer cells enhanced STING signaling in cells that engulfed such dying cells, promoting immune activation (Ahn et al., 2018).

A recent report showed that the increase of cytoplasmic dsDNA upon radiotherapy depends on the dose of radiation used; doses >10–12 Gy induce expression of the DNA exonuclease TREX1, resulting in degradation of cytoplasmic dsDNA in three different cancer cell lines (TSA, MC38, and 4T1) and reduced immunogenicity (Vanpouille-Box et al., 2017). In contrast, we found a comparable increase of cytoplasmic dsDNA after irradiation with 8 or 20 Gy as well as exposition to 15 μM cisplatin in CT26. We currently lack an explanation for this discrepancy. Furthermore, we showed that therapeutic efficacy of radiotherapy given as a single dose of 20 Gy was decreased in cGAS-deficient CT26 tumors when compared to cGAS-proficient tumors.

We can offer at least two explanations for our observation that cGAS-expressing cancers respond better to genotoxic treatment. First, therapy-induced increase of cytoplasmic dsDNA may translate directly in production of more cGAMP and type I IFN, thus providing a stronger immune stimulus. However, untreated cancer cells already contain at least 10-fold more cytoplasmic dsDNA than untransformed cells, and we do not know whether a further 2- to 4-fold increase by genotoxic therapy significantly adds to immune stimulation. Second, genotoxic therapies, and perhaps all therapies that involve concomitant immune stimulation, may work better when tumors are hot at the start of therapy. Indeed, some studies show that immune checkpoint inhibitors work better if cancer cells contain substantial amounts of cytoplasmic dsDNA (Vanpouille-Box et al., 2017) or if they are combined with intratumoral application of STING agonists (Wang et al., 2017; Ager et al., 2017).

Tumor-infiltrating effector $CD8^+$ T cells mediate the clinical response to immune checkpoint inhibitors. Therefore, hot tumors respond better to immune checkpoint inhibition (Ayers et al., 2017; Van Allen et al., 2015). cGAS-expressing tumors responded significantly better to anti-PD1 and anti-CTLA4 treatment than cGAS-deficient tumors, which is in line with our observation that cancer-cell-intrinsic cGAS promotes infiltration by effector $CD8^+$ T cells that can be targeted by immune checkpoint inhibition.

Despite the wealth of evidence for cGAS/STING supporting anti-tumor immunity, there are reports showing a detrimental role of this pathway. First, STING was shown to promote the growth of poorly immunogenic tumors via indolamine 2,3 dioxygenase (IDO) activation (Lemos et al., 2016). This study used mostly LLC and EL-4 cancer cells, and we showed here that LLCs contain low amounts of cGAS, which may explain their low immunogenicity. The authors did not address, however, how STING drives IDO production and subsequent suppression of $CD8^+$ T cells. Second, it was shown that chromosomal instability leads to micronuclei, increased amounts of cytoplasmic dsDNA, activation of the cGAS/STING pathway, and increased metastasis (Bakhoum et al., 2018). Most of the experiments used xenografted human cancer cells, thus precluding involvement of the immune system. Third, STING-deficient mice are resistant to inflammation-driven skin squamous cell carcinoma (Ahn et al., 2014), which may not be representative of most cancers. Fourth, metastatic cells in the brain establish gap junctions with astrocytes to transfer cGAMP. The resulting, STING-dependent production of pro-inflammatory cytokines supports proliferation of metastasized cells and makes them chemoresistant (Chen et al., 2016). Thus, in a particular context, the cGAS/STING pathway may promote cancer.

In summary, together with the recent report by Marcus et al. (2018), our results propose that cancer-cell-intrinsic cGAS is essential to tumor control by innate as well as adaptive immunity. Thus, cGAS expression makes tumors hot and may serve as a useful biomarker for immunogenicity and presumably also for responsiveness to (immune) therapy.

STAR★METHODS

Detailed methods are provided in the online version of this paper and include the following:

- KEY RESOURCES TABLE
- LEAD CONTACT AND MATERIALS AVAILABILITY
- EXPERIMENTAL MODEL AND SUBJECT DETAILS
  - Mouse strains
  - Cell lines
  - Colorectal adenocarcinoma paraffin sections
- METHOD DETAILS
  - Modification of cell lines
  - Measurement of cGAS and STING in tumor cell lines
  - Co-culture experiments
  - *In vivo* tumor experiments and treatments
  - Flow cytometry
  - Western blotting
  - Quantification of type I IFN
  - Quantification of cytoplasmic DNA
  - Quantification of cytokines in tumor lysates
  - Four-color immunofluorescence
  - Calcein AM transfer assay
  - Quantification of gamma-H2AX
  - Colony-forming assay
- QUANTIFICATION AND STATISTICAL ANALYSIS
  - Quantification of immunofluorescence data
  - Statistical analysis
- DATA AND CODE AVAILABILITY

SUPPLEMENTAL INFORMATION

Supplemental Information can be found online at https://doi.org/10.1016/j.celrep.2019.09.065.

ACKNOWLEDGMENTS

We thank Giancarlo Marra (University of Zurich, Switzerland) for providing the colorectal adenocarcinoma paraffin slides and determining the microsatellite instability status of the patients. We thank Anne Müller, Carla Rohrer-Bley, Christian Münz, Burkhard Becher (all University of Zurich, Switzerland), and Holger Moch and Achim Weber (both University Hospital Zurich) for valuable input and support. We thank the personnel from the Laboratory Animal Service Center (University of Zurich) for expert animal care. This work was financially supported by the Swiss National Science Foundation (SNSF), the Swiss Cancer League (Oncosuisse), the Science Foundation for Oncology (SFO), the Hartmann-Müller Foundation, the Helmut-Horten Foundation, the University Research Priority Program (URPP) "Translational Cancer Research," and the Czech Science Foundation (17-02080S).

AUTHOR CONTRIBUTIONS

L.S., M.v.d.B., C.S., and S.S. conceived experiments; L.S., C.S., E.G., V.C., S.S., N.A.S., K.S., G.L., and Z.N. performed experiments; L.S. and M.v.d.B. wrote the manuscript; W.B. and H.Y. provided essential reagents; and M.v.d.B. secured funding.

DECLARATION OF INTERESTS

The authors declare no competing interests.

Received: November 30, 2018
Revised: August 5, 2019
Accepted: September 20, 2019
Published: October 29, 2019

REFERENCES

Ablasser, A., and Chen, Z.J. (2019).). CGAS in action: expanding roles in immunity and inflammation. Science *363*, eaat8657.

Ablasser, A., Goldeck, M., Cavlar, T., Deimling, T., Witte, G., Röhl, I., Hopfner, K.P., Ludwig, J., and Hornung, V. (2013a). cGAS produces a 2′-5′-linked cyclic dinucleotide second messenger that activates STING. Nature *498*, 380–384.

Ablasser, A., Schmid-Burgk, J.L., Hemmerling, I., Horvath, G.L., Schmidt, T., Latz, E., and Hornung, V. (2013b). Cell intrinsic immunity spreads to bystander cells via the intercellular transfer of cGAMP. Nature *503*, 530–534.

Ager, C.R., Reilley, M.J., Nicholas, C., Bartkowiak, T., Jaiswal, A.R., and Curran, M.A. (2017). Intratumoral STING activation with T-cell checkpoint modulation generates systemic antitumor immunity. Cancer Immunol. Res. *5*, 676–684.

Ahn, J., Xia, T., Konno, H., Konno, K., Ruiz, P., and Barber, G.N. (2014). Inflammation-driven carcinogenesis is mediated through STING. Nat. Commun. *5*, 5166.

Ahn, J., Xia, T., Rabasa Capote, A., Betancourt, D., and Barber, G.N. (2018). Extrinsic phagocyte-dependent STING signaling dictates the immunogenicity of dying cells. Cancer Cell *33*, 862–873.e5.

Ayers, M., Lunceford, J., Nebozhyn, M., Murphy, E., Loboda, A., Kaufman, D.R., Albright, A., Cheng, J.D., Kang, S.P., Shankaran, V., et al. (2017). IFN-γ-related mRNA profile predicts clinical response to PD-1 blockade. J. Clin. Invest. *127*, 2930–2940.

Baird, J.R., Friedman, D., Cottam, B., Dubensky, T.W., Jr., Kanne, D.B., Bambina, S., Bahjat, K., Crittenden, M.R., and Gough, M.J. (2016). Radiotherapy combined with novel STING-targeting oligonucleotides results in regression of established tumors. Cancer Res. *76*, 50–61.

Bakhoum, S.F., Ngo, B., Laughney, A.M., Cavallo, J.A., Murphy, C.J., Ly, P., Shah, P., Sriram, R.K., Watkins, T.B.K., Taunk, N.K., et al. (2018). Chromosomal instability drives metastasis through a cytosolic DNA response. Nature *553*, 467–472.

Binnewies, M., Roberts, E.W., Kersten, K., Chan, V., Fearon, D.F., Merad, M., Coussens, L.M., Gabrilovich, D.I., Ostrand-Rosenberg, S., Hedrick, C.C., et al. (2018). Understanding the tumor immune microenvironment (TIME) for effective therapy. Nat. Med. *24*, 541–550.

Biron, C.A., Nguyen, K.B., Pien, G.C., Cousens, L.P., and Salazar-Mather, T.P. (1999). Natural killer cells in antiviral defense: function and regulation by innate cytokines. Annu. Rev. Immunol. *17*, 189–220.

Broz, M.L., Binnewies, M., Boldajipour, B., Nelson, A.E., Pollack, J.L., Erle, D.J., Barczak, A., Rosenblum, M.D., Daud, A., Barber, D.L., et al. (2014). Dissecting the tumor myeloid compartment reveals rare activating antigen-presenting cells critical for T cell immunity. Cancer Cell *26*, 638–652.

Burnette, B.C., Liang, H., Lee, Y., Chlewicki, L., Khodarev, N.N., Weichselbaum, R.R., Fu, Y.X., and Auh, S.L. (2011). The efficacy of radiotherapy relies upon induction of type i interferon-dependent innate and adaptive immunity. Cancer Res. *71*, 2488–2496.

Chen, D.S., and Mellman, I. (2017). Elements of cancer immunity and the cancer-immune set point. Nature *541*, 321–330.

Chen, Q., Boire, A., Jin, X., Valiente, M., Er, E.E., Lopez-Soto, A., Jacob, L., Patwa, R., Shah, H., Xu, K., et al. (2016). Carcinoma-astrocyte gap junctions promote brain metastasis by cGAMP transfer. Nature *533*, 493–498.

Corrales, L., Glickman, L.H., McWhirter, S.M., Kanne, D.B., Sivick, K.E., Katibah, G.E., Woo, S.R., Lemmens, E., Banda, T., Leong, J.J., et al. (2015). Direct activation of STING in the tumor microenvironment leads to potent and systemic tumor regression and immunity. Cell Rep. *11*, 1018–1030.

Dai, P., Wang, W., Yang, N., Serna-Tamayo, C., Ricca, J.M., Zamarin, D., Shuman, S., Merghoub, T., Wolchok, J.D., and Deng, L. (2017). Intratumoral delivery of inactivated modified vaccinia virus Ankara (IMVA) induces systemic antitumor immunity via STING and Batf3-dependent dendritic cells. Sci. Immunol. *2*, eaal1713.

Deng, L., Liang, H., Xu, M., Yang, X., Burnette, B., Arina, A., Li, X.D., Mauceri, H., Beckett, M., Darga, T., et al. (2014). STING-dependent cytosolic DNA sensing promotes radiation-induced type I interferon-dependent antitumor immunity in immunogenic tumors. Immunity *41*, 843–852.

Diamond, M.S., Kinder, M., Matsushita, H., Mashayekhi, M., Dunn, G.P., Archambault, J.M., Lee, H., Arthur, C.D., White, J.M., Kalinke, U., et al. (2011). Type I interferon is selectively required by dendritic cells for immune rejection of tumors. J. Exp. Med. *208*, 1989–2003.

Dunn, G.P., Koebel, C.M., and Schreiber, R.D. (2006). Interferons, immunity and cancer immunoediting. Nat. Rev. Immunol. *6*, 836–848.

Fenech, M., Kirsch-Volders, M., Natarajan, A.T., Surralles, J., Crott, J.W., Parry, J., Norppa, H., Eastmond, D.A., Tucker, J.D., and Thomas, P. (2011). Molecular mechanisms of micronucleus, nucleoplasmic bridge and nuclear bud formation in mammalian and human cells. Mutagenesis *26*, 125–132.

Franken, N.A., Rodermond, H.N., Stap, J., Haveman, J., and van Bree, C. (2006). Clonogenic assay of cells in vitro. Nat. Protoc. *1*, 2315–2319.

Fuertes, M.B., Kacha, A.K., Kline, J., Woo, S.R., Kranz, D.M., Murphy, K.M., and Gajewski, T.F. (2011). Host type I IFN signals are required for antitumor CD8+ T cell responses through CD8alpha+ dendritic cells. J. Exp. Med. *208*, 2005–2016.

Gajewski, T.F., Schreiber, H., and Fu, Y.X. (2013). Innate and adaptive immune cells in the tumor microenvironment. Nat. Immunol. *14*, 1014–1022.

Galluzzi, L., Buqué, A., Kepp, O., Zitvogel, L., and Kroemer, G. (2017). Immunogenic cell death in cancer and infectious disease. Nat. Rev. Immunol. *17*, 97–111.

Galon, J., Costes, A., Sanchez-Cabo, F., Kirilovsky, A., Mlecnik, B., Lagorce-Pagès, C., Tosolini, M., Camus, M., Berger, A., Wind, P., et al. (2006). Type, density, and location of immune cells within human colorectal tumors predict clinical outcome. Science *313*, 1960–1964.

Gao, P., Ascano, M., Wu, Y., Barchet, W., Gaffney, B.L., Zillinger, T., Serganov, A.A., Liu, Y., Jones, R.A., Hartmann, G., et al. (2013). Cyclic [G(2′,5′)pA(3′,5′)p] is the metazoan second messenger produced by DNA-activated cyclic GMP-AMP synthase. Cell *153*, 1094–1107.

Gupta, A., Probst, H.C., Vuong, V., Landshammer, A., Muth, S., Yagita, H., Schwendener, R., Pruschy, M., Knuth, A., and van den Broek, M. (2012). Radiotherapy promotes tumor-specific effector CD8$^+$ T cells via dendritic cell activation. J. Immunol. *189*, 558–566.

Harding, S.M., Benci, J.L., Irianto, J., Discher, D.E., Minn, A.J., and Greenberg, R.A. (2017). Mitotic progression following DNA damage enables pattern recognition within micronuclei. Nature *548*, 466–470.

Härtlova, A., Erttmann, S.F., Raffi, F.A., Schmalz, A.M., Resch, U., Anugula, S., Lienenklaus, S., Nilsson, L.M., Kröger, A., Nilsson, J.A., et al. (2015). DNA damage primes the type I interferon system via the cytosolic DNA sensor STING to promote anti-microbial innate immunity. Immunity *42*, 332–343.

Huang, A.Y., Gulden, P.H., Woods, A.S., Thomas, M.C., Tong, C.D., Wangt, W., Engelhardt, V.H., et al. (1996). The immunodominant major histocompatibility complex class I-restricted antigen of a murine colon tumor derives from an endogenous retroviral gene product. Proc. Natl. Acad. Sci. USA *93*, 9730–9735.

Inaba, K., Inaba, M., Romani, N., Aya, H., Deguchi, M., Ikehara, S., Muramatsu, S., and Steinman, R.M. (1992). Generation of large numbers of dendritic cells from mouse bone marrow cultures supplemented with granulocyte/macrophage colony-stimulating factor. J. Exp. Med. *176*, 1693–1702.

Ishikawa, H., and Barber, G.N. (2008). STING is an endoplasmic reticulum adaptor that facilitates innate immune signalling. Nature *455*, 674–678.

Ishikawa, H., Ma, Z., and Barber, G.N. (2009). STING regulates intracellular DNA-mediated, type I interferon-dependent innate immunity. Nature *461*, 788–792.

Kitai, Y., Kawasaki, T., Sueyoshi, T., Kobiyama, K., Ishii, K.J., Zou, J., Akira, S., Matsuda, T., and Kawai, T. (2017). DNA-containing exosomes derived from cancer cells treated with topotecan activate a STING-dependent pathway and reinforce antitumor immunity. J. Immunol. *198*, 1649–1659.

Klarquist, J., Hennies, C.M., Lehn, M.A., Reboulet, R.A., Feau, S., and Janssen, E.M. (2014). STING-mediated DNA sensing promotes antitumor and autoimmune responses to dying cells. J. Immunol. *193*, 6124–6134.

Lemos, H., Mohamed, E., Huang, L., Ou, R., Pacholczyk, G., Arbab, A.S., Munn, D., and Mellor, A.L. (2016). STING promotes the growth of tumors characterized by low antigenicity via IDO activation. Cancer Res. *76*, 2076–2081.

Li, T., and Chen, Z.J. (2018). The cGAS-cGAMP-STING pathway connects DNA damage to inflammation, senescence, and cancer. J. Exp. Med. *215*, 1287–1299.

Li, T., Cheng, H., Yuan, H., Xu, Q., Shu, C., Zhang, Y., Xu, P., Tan, J., Rui, Y., Li, P., and Tan, X. (2016). Antitumor activity of cGAMP via stimulation of cGAS-cGAMP-STING-IRF3 mediated innate immune response. Sci. Rep. *6*, 19049.

Lienenklaus, S., Cornitescu, M., Ziętara, N., Łyszkiewicz, M., Gekara, N., Jabłónska, J., Edenhofer, F., Rajewsky, K., Bruder, D., Hafner, M., et al. (2009). Novel reporter mouse reveals constitutive and inflammatory expression of IFN-β in vivo. J. Immunol. *183*, 3229–3236.

Mackenzie, K.J., Carroll, P., Martin, C.A., Murina, O., Fluteau, A., Simpson, D.J., Olova, N., Sutcliffe, H., Rainger, J.K., Leitch, A., et al. (2017). cGAS surveillance of micronuclei links genome instability to innate immunity. Nature *548*, 461–465.

Marcus, A., Mao, A.J., Lensink-Vasan, M., Wang, L., Vance, R.E., and Raulet, D.H. (2018). Tumor-derived cGAMP triggers a STING-mediated interferon response in non-tumor cells to activate the NK cell response. Immunity *49*, 754–763.e4.

Ramanjulu, J.M., Pesiridis, G.S., Yang, J., Concha, N., Singhaus, R., Zhang, S.Y., Tran, J.L., Moore, P., Lehmann, S., Eberl, H.C., et al. (2018). Design of amidobenzimidazole STING receptor agonists with systemic activity. Nature *564*, 439–443.

Saccheri, F., Pozzi, C., Avogadri, F., Barozzi, S., Faretta, M., Fusi, P., and Rescigno, M. (2010). Bacteria-induced gap junctions in tumors favor antigen cross-presentation and antitumor immunity. Sci. Transl. Med. *2*, 44ra57.

Scheu, S., Dresing, P., and Locksley, R.M. (2008). Visualization of IFNbeta production by plasmacytoid versus conventional dendritic cells under specific stimulation conditions in vivo. Proc. Natl. Acad. Sci. USA *105*, 20416–20421.

Shen, Y.J., Le Bert, N., Chitre, A.A., Koo, C.X., Nga, X.H., Ho, S.S., Khatoo, M., Tan, N.Y., Ishii, K.J., and Gasser, S. (2015). Genome-derived cytosolic DNA mediates type I interferon-dependent rejection of B cell lymphoma cells. Cell Rep. *11*, 460–473.

Sheng, W., LaFleur, M.W., Nguyen, T.H., Chen, S., Chakravarthy, A., Conway, J.R., Li, Y., Chen, H., Yang, H., Hsu, P.H., et al. (2018). LSD1 ablation stimulates anti-tumor immunity and enables checkpoint blockade. Cell *174*, 549–563.e19.

Siliņa, K., Burkhardt, C., Casanova, R., Solterman, A., and van den Broek, M. (2018a). A quantitative pathology approach to analyze the development of human cancer-associated tertiary lymphoid structures. Methods Mol. Biol. *1845*, 71–86.

Siliņa, K., Soltermann, A., Attar, F.M., Casanova, R., Uckeley, Z.M., Thut, H., Wandres, M., Isajevs, S., Cheng, P., Curioni-Fontecedro, A., et al. (2018b). Germinal centers determine the prognostic relevance of tertiary lymphoid structures and are impaired by corticosteroids in lung squamous cell carcinoma. Cancer Res. *78*, 1308–1320.

Simoni, Y., Becht, E., Fehlings, M., Loh, C.Y., Koo, S.L., Teng, K.W.W., Yeong, J.P.S., Nahar, R., Zhang, T., Kared, H., et al. (2018). Bystander CD8$^+$ T cells are abundant and phenotypically distinct in human tumour infiltrates. Nature *557*, 575–579.

Sistigu, A., Yamazaki, T., Vacchelli, E., Chaba, K., Enot, D.P., Adam, J., Vitale, I., Goubar, A., Baracco, E.E., Remédios, C., et al. (2014). Cancer cell-autonomous contribution of type I interferon signaling to the efficacy of chemotherapy. Nat. Med. *20*, 1301–1309.

Song, S., Peng, P., Tang, Z., Zhao, J., Wu, W., Li, H., Shao, M., Li, L., Yang, C., Duan, F., et al. (2017). Decreased expression of STING predicts poor prognosis in patients with gastric cancer. Sci. Rep. *7*, 39858.

Stetson, D.B., and Medzhitov, R. (2006). Recognition of cytosolic DNA activates an IRF3-dependent innate immune response. Immunity *24*, 93–103.

Sun, L., Wu, J., Du, F., Chen, X., and Chen, Z.J. (2013). Cyclic GMP-AMP synthase is a cytosolic DNA sensor that activates the type I interferon pathway. Science *339*, 786–791.

Surace, L., Lysenko, V., Fontana, A.O., Cecconi, V., Janssen, H., Bicvic, A., Okoniewski, M., Pruschy, M., Dummer, R., Neefjes, J., et al. (2015). Complement is a central mediator of radiotherapy-induced tumor-specific immunity and clinical response. Immunity *42*, 767–777.

Swann, J.B., Hayakawa, Y., Zerafa, N., Sheehan, K.C.F., Scott, B., Schreiber, R.D., Hertzog, P., and Smyth, M.J. (2007). Type I IFN contributes to NK cell homeostasis, activation, and antitumor function. J. Immunol. *178*, 7540–7549.

Uzé, G., Di Marco, S., Mouchel-Vielh, E., Monneron, D., Bandu, M.T., Horisberger, M.A., Dorques, A., Lutfalla, G., and Mogensen, K.E. (1994). Domains of interaction between alpha interferon and its receptor components. J. Mol. Biol. *243*, 245–257.

Van Allen, E.M., Miao, D., Schilling, B., Shukla, S.A., Blank, C., Zimmer, L., Sucker, A., Hillen, U., Foppen, M.H.G., Goldinger, S.M., et al. (2015). Genomic correlates of response to CTLA-4 blockade in metastatic melanoma. Science *350*, 207–211.

van der Woude, L.L., Gorris, M.A.J., Halilovic, A., Figdor, C.G., and de Vries, I.J.M. (2017). Migrating into the tumor: a roadmap for T Cells. Trends Cancer *3*, 797–808.

Vanpouille-Box, C., Alard, A., Aryankalayil, M.J., Sarfraz, Y., Diamond, J.M., Schneider, R.J., Inghirami, G., Coleman, C.N., Formenti, S.C., and Demaria, S. (2017). DNA exonuclease Trex1 regulates radiotherapy-induced tumour immunogenicity. Nat. Commun. *8*, 15618.

Vanpouille-Box, C., Demaria, S., Formenti, S.C., and Galluzzi, L. (2018). Cytosolic DNA sensing in organismal tumor control. Cancer Cell *34*, 361–378.

Wang, H., Hu, S., Chen, X., Shi, H., Chen, C., Sun, L., and Chen, Z.J. (2017). cGAS is essential for the antitumor effect of immune checkpoint blockade. Proc. Natl. Acad. Sci. USA *114*, 1637–1642.

Woo, S.R., Fuertes, M.B., Corrales, L., Spranger, S., Furdyna, M.J., Leung, M.Y.K., Duggan, R., Wang, Y., Barber, G.N., Fitzgerald, K.A., et al. (2014). STING-dependent cytosolic DNA sensing mediates innate immune recognition of immunogenic tumors. Immunity *41*, 830–842.

Wu, J., Sun, L., Chen, X., Du, F., Shi, H., Chen, C., and Chen, Z.J. (2013). Cyclic GMP-AMP is an endogenous second messenger in innate immune signaling by cytosolic DNA. Science *339*, 826–830.

Xia, T., Konno, H., Ahn, J., and Barber, G.N. (2016). Deregulation of STING signaling in colorectal carcinoma constrains DNA damage responses and correlates with tumorigenesis. Cell Rep. *14*, 282–297.

Yang, C.A., Huang, H.Y., Chang, Y.S., Lin, C.L., Lai, I.L., and Chang, J.G. (2017). DNA-sensing and nuclease gene expressions as markers for colorectal cancer progression. Oncology *92*, 115–124.

STAR★METHODS

KEY RESOURCES TABLE

REAGENT or RESOURCE	SOURCE	IDENTIFIER
Antibodies		
STING	Cell Signaling Technology	Clone D2P2F; 13647S; RRID:AB_2732796
cGAS	Cell Signaling Technology	Clone D3O8O; 31659S; RRID:AB_2799008
CX43	Cell Signaling Technology	Clone 3512; 3512S; RRID:AB_2294590
Alpha-tubulin	Cell Signaling Technology	Clone DM1A; 3873S; RRID:AB_1904178
Beta-actin	Sigma	Clone AC-15; A5441; RRID:AB_476744
HRP-goat-anti-mouse IgG	BioLegend	Poly4053; RRID:AB_315009
HRP-goat-anti-rabbit IgG	Dianova	111-035-008; RRID:AB_2337937
cGAS	Cell Signaling Technology	Clone D1D3G; 15102S; RRID:AB_2732795
CD8	Bio-Rad	4B11; MCA1817T; RRID:AB_322868
Pan-Cytokeratin	Santa Cruz	Clone h-240; sc-15367; RRID:AB_2134438
HRP-donkey-anti-rabbit IgG	Jackson ImmunoResearch	711-035-152; RRID:AB_10015282
HRP-donkey-anti-rat IgG	Jackson ImmunoResearch	712-035-153; RRID:AB_2340639
AlexaFluor 568-goat-anti-mouse IgG	Life Technologies	A11031; RRID:AB_144696
gamma-H2AX	Millipore	05-636; RRID:AB_309864
CD11b – FITC	BioLegend	Clone M1/70; 101206; RRID:AB_213789
NK1.1 – FITC	BioLegend	Clone PK136; 108706; RRID:AB_313393
CD4 – PE	BioLegend	Clone GK1.5; 100408; RRID:AB_312693
CD45.2 – PerCP/Cy5.5	BioLegend	Clone 104; 109828; RRID:AB_893350
CD45.2 – APC	BioLegend	Clone 104; 109814; RRID:AB_389211
IFNgammma – PE/Cy7	BioLegend	Clone XMG1.2; 505826; RRID:AB_2295770
CD8a – BV605	BioLegend	Clone 53-6.7; 100744; RRID:AB_2562609
CD3e – APC	BioLegend	Clone 17A2; 100236; RRID:AB_2561456
FoxP3 – APC	eBioscience	Clone FJK-16 s; 17-5773-80; RRID:AB_469456
CD8a – APC	BioLegend	Clone 53-6.7; 100712; RRID:AB_312751
CD4 – APC/Cy7	BioLegend	Clone GK1.5; 100414; RRID:AB_312699
CD3e – APC/Cy7	BioLegend	Clone 17A2; 100222; RRID:AB_2242784
CD11c – BV650	BioLegend	Clone N418; 117339; RRID:AB_2562414
CD45.2 – BV605	BioLegend	Clone 104; 109841; RRID:AB_2563485
CD11b – BV510	BioLegend	Clone M1/70; 101245; RRID:AB_2561390
F4/80 – PB	BioLegend	Clone BM8; 123124; RRID:AB_893475
F4/80 – BV421	BioLegend	Clone BM8; 123132; RRID:AB_11203717
CD31 – FITC	BioLegend	Clone 390; 102406; RRID:AB_312901
MHC-II – PE/Cy7	BioLegend	Clone M5/114.15.2; 107630; RRID:AB_493528
CD122-PE	BioLegend	Clone TM-beta 1; 123210; RRID:AB_940617
NKp46-PerCP/eFluor 710	eBioscience	Clone 29A1.4; 46335182; RRID:AB_1834441
CD3- PE/Cy7	BioLegend	Clone 145-2C11; 100320; RRID:AB_312685
CD45-PB	BioLegend	Clone 104 Mouse; 109820; RRID:AB_492872
CD49b-APC	BioLegend	Clone DX5; 108910; RRID:AB_313415
CD39-PerCP/eFluor 710	eBioscience	Clone 24DMS1; 46039182; RRID:AB_10717953
CD103 PE	BioLegend	Clone 2E7; 121405; RRID:AB_535948
Zombie Violet Fixable Viability Kit	BioLegend	423114
Zombie NIR Fixable Viability Kit	BioLegend	423106

(*Continued on next page*)

Continued

REAGENT or RESOURCE	SOURCE	IDENTIFIER
Biological Samples		
Tissue microarray of 120 colorectal adenocarcinoma samples	Department of Pathology and Molecular Pathology, University Hospital Zurich, Switzerland	N/A
Paraffin sections of colorectal adenocarcinoma samples with determined MSI status	Triemli Hospital Zurich	N/A
Chemicals, Peptides, and Recombinant Proteins		
Recombinant mouse IFN-beta	Sigma-Aldrich	I9032-1VL
Polyethylenimine (PEI)	Polysciences	23966-1
Cisplatin	Sandoz	L01XA01
Matrigel	Corning	354234
Zombie-Violet fixable viability stain	BioLegend	423114
Zombie-NIR fixable viability stain	BioLegend	423106
PMA	Sigma	P1585-1MG
Ionomycin	Sigma	I0634-1MG
Brefeldin A	Sigma	B6542-25MG
AH-1 peptide (SPSYVYHQF)	PolyPeptide Laboratories	N/A
FoxP3/Transcription factor staining buffer set	eBioscience	00-5523-00
Opal 520	PerkinElmer	FP1487001KT
Opal 540	PerkinElmer	FP1494001KT
Opal 620	PerkinElmer	FP1495001KT
Opal 650	PerkinElmer	FP1496001KT
Opal 690	PerkinElmer	FP1497001KT
1X Plus Amplification Diluent	PerkinElmer	FP1498
Anti-PD1	Hideo Yagita, Tokyo, Japan	RMP1-14
Anti-CTLA4	Jim Allison, Texas, US	9H10
Calcein, AM, cell-permanent dye	Invitrogen	C3100MP
Poly-L-lysine (0.1%)	Sigma Aldrich	P8920
Critical Commercial Assays		
Prime Flow RNA assay	ThermoFisher	88-18005-210
Prime Flow IFNb1	ThermoFisher	PF210 (VB10-3282108-PF)
Mouse IFN-beta ELISA	PBL Assay Science	42410-1
Luciferase 1000 assay system	Promega	E4550
NE-PER Nuclear and cytoplasmic Extraction Reagents	ThermoFisher	78833
AccuClear Nano dsDNA Assay kit	Molecular Devices	R3650A
LEGENDplex Mouse Inflammation Panel	BioLegend	740150
Experimental Models: Cell Lines		
4T07	Gerhard Christofori, Basel, Switzerland	N/A
4T1	Burkhard Becher, Zurich, Switzerland	N/A
B16BL6	Lubor Borsig, Zurich, Switzerland	N/A
B16F10	ATCC	CRL-6475
CMS5a	Hiroyoshi Nishikawa, Osaka, Japan	N/A
CT26	ATCC	CRL-2638
LL171	Roman Spörri, ETHZ, Switzerland	N/A
LLC	ATCC	CRL-1642
MC38	Mark Smyth, Brisbane, Australia	N/A
MC57	Rolf Zinkernagel, Zurich, Switzerland	N/A

(*Continued on next page*)

Continued

REAGENT or RESOURCE	SOURCE	IDENTIFIER
RN5	Emanuela Felley-Bosco, Zurich, Switzerland	N/A
CT26$^{\Delta Mb21d1}$	This paper	N/A
CT26$^{\Delta Tmem173}$	This paper	N/A
CT26$^{\Delta Gja1}$	This paper	N/A
CT26^{Ctrl}	This paper	N/A
LLC^{Mb21d1}	This paper	N/A
X63-mGM-CSF	Manfred Kopf, Zurich, Switzerland	N/A
Experimental Models: Organisms/Strains		
BALB/cRj1	Janvier	N/A
C57BL/6NRj	Janvier	N/A
B6(C)-*Cgas*$^{tm1d(EUCOMM)Hmgu}$/J	The Jackson Laboratory	026554
NOD.Cg-*Prkdc*^{scid}*Il2rg*^{tm1Wjl}/SzJ	The Jackson Laboratory	013062
C57BL/6J-*Tmem173*^{Gt}/J	The Jackson Laboratory	017537
B6.129S2-*Ifnar1*^{tm1Agt}/Mmjax	The Jackson Laboratory	32045-JAX
Oligonucleotides		
Primers for CRISPR/Cas9 genomic editing, see Table S1	This paper	N/A
Recombinant DNA		
pSpCas9(BB)-2A-GFP	Addgene	PX458; 48138
pLenti-EF1α-Flag-mm-cGas	Winfried Barchet, Bonn, Germany	N/A
pMD2.G	Addgene	12259
pCMV-dR8.91	Christian Münz, Zurich, Switzerland	N/A
Software and Algorithms		
Prism	GraphPad Prism software	Version 7.0
FlowJo	Tree Star software	Version 10.1
inForm	PerkinElmer	CLS1355781
ImageJ	Fiji	N/A
Other		
Irradiation unit	RADSOURCE	RS2000
FastPrep tissue homogenizer	MPBiomedicals	N/A
Zirconium beads	Precellys	BER103BK
Multispectral microscopy system Vectra 3.0	PerkinElmer	N/A
SpectraMax i3	Molecular Devices	N/A
DM6 B fluorescent microscope	Leica Biosystems	N/A
IX83 microscope	Olympus	N/A
Scan R imaging platform	Olympus	N/A

LEAD CONTACT AND MATERIALS AVAILABILITY

Further information and requests for resources and reagents should be directed to and fulfilled by the Lead Contact, Dr. Maries van den Broek (vandenbroek@immunology.uzh.ch).

All unique/stable reagents generated in this study are available from the Lead Contact with a completed Materials Transfer Agreement.

EXPERIMENTAL MODEL AND SUBJECT DETAILS

Mouse strains

BALB/cRj1 and C57BL/6NRj mice were purchased from Janvier and cGAS-deficient (cGAS$^{-/-}$, B6(C)-*Cgas*$^{tm1d(EUCOMM)Hmgu}$/J) mice were purchased from Jackson Laboratory. NOD.Cg-*Prkdc*^{scid}*Il2rg*^{tm1Wjl}/SzJ (NSG) mice were originally obtained from the Jackson

Laboratory and provided by Christian Münz, University of Zurich, Switzerland. Femora and tibiae from STING-deficient (C57BL/6J-*Tmem173*^{Gt}/J; *Tmem173*^{Gt}) mice were provided by Winfried Barchet, University of Bonn, Germany. All mice were kept and bred under pathogen-free conditions at the Laboratory Animal Services Center at the University of Zurich. All experiments were performed with 8-12-weeks-old female mice, unless stated otherwise. All animal experiments were approved by the Cantonal Veterinary Office Zurich under the license number 084/2015 and 140/2018 and performed according to cantonal and federal regulations.

Cell lines

CT26, LLC, 4T1, B16F10, B16BL6, MC38, MC57, CMS5a and 4T07 provided by were cultured in Dulbecco's modified Eagle's medium (DMEM, GIBCO) supplemented with 5% fetal calf serum (FCS, Thermo Fisher Scientific), 30 U/ml Penicillin, 30 μg/ml Streptomycin (antibiotics, Thermo Fisher Scientific) and 2 mM L-Glutamine (Thermo Fisher Scientific). RN5 cells were cultured in DMEM/F-12 (1:1) medium (Thermo Fisher Scientific) supplemented with 15% FCS, 0.1 mM 2-mercaptoethanol (Sigma Aldrich), 1% MEM non-essential amino acids (Thermo Fisher Scientific) and 100 mM sodium pyruvate (Thermo Fisher Scientific) and antibiotics. LL171 (Uzé et al., 1994) were cultured in Roswell Park Memorial Institute (RPMI) 1640 medium (GIBCO) supplemented with 10% FCS, L-Glutamine and antibiotics. CT26 *Mb21d1*-, *Tmem173*- or *Gja1*-deficient cells, and LLC *Mb21d1*-overexpressing cells were generated and cultured as described above.

All cell lines were tested negative for a number of pathogens including *Mycoplasma* ssp. by PCR.

Colorectal adenocarcinoma paraffin sections

Tumor tissues from patients with colorectal adenocarcinoma of the proximal colon were collected at the Triemli Hospital Zurich, Switzerland. Donors provided written, informed consent to tissue collection, analysis and data publication. Law abidance was reviewed and approved by the ethics commission of the Canton Zurich (KEK-ZH-2015-0068 and KEK-ZH-2013-0584). Samples were numerically coded to protect donors' rights to confidentiality and privacy. The microsatellite-instability (MSI) status was determined by immunohistochemical detection of MLH1 and MLH2. We analyzed 25 patients with MS-stable disease.

METHOD DETAILS

Modification of cell lines

Mb21d1 (cGAS), *Tmem173* (STING) or *Gja1* (CX43) genes were targeted in CT26 cells using CRISPR/Cas9. Per gene, three guide-RNAs (gRNAs) were designed (Table S1), of which two were paired per transfection. gRNAs were cloned into the pSpCas9(BB)-2A-GFP vector. CT26 cells were transfected with polyethyleneimine (PEI) and 2000 ng of two PX458-gRNA expression plasmids per target gene. GFP^{+} cells were FACS-sorted using a FACSARIA III (BD Biosciences) and cloned by limiting dilution. Absence of target gene was confirmed in cGAS-deficient CT26 (CT26$^{\Delta Mb21d1}$), STING-deficient CT26 (CT26$^{\Delta Tmem173}$) and CX43-deficient CT26 (CT26$^{\Delta Gja1}$) by Western Blot. In order to avoid potential single-clone-dependent artifacts, oligoclonal cell lines were generated as follows. Five clones with determined deficiency of target gene were mixed in equal parts and used for experiments. The control CT26 cell line (CT26^{ctrl}) was generated as described above using the empty PX458 vector.

To overexpress cGAS, we used the lentiviral plasmid pLenti-EF1α-Flag-mm-cGAS. Lentiviral particles were generated using a second-generation lentiviral packaging system consisting of pMD2.G and pCMV-dR8.91. LLC cells were transduced and subsequently cultured in DMEM supplemented with 2 μg/ml puromycin (Invitrogen, #A11138-03) to select transduced cells. cGAS overexpression was confirmed by Western Blot.

Measurement of cGAS and STING in tumor cell lines

Tumor cells (1.5x10^{6}) were seeded in T175 flasks, cultured for 24 h and expression of cGAS and STING was quantified by Western Blot.

To assess the function of cGAS and STING, 3x10^{5} tumor cells/well were seeded in 24-well plates. Tumor cells were transfected with 1 μg genomic DNA extracted from CT26 cells using PEI. Cells were incubated overnight at 37°C and type I IFNs were quantified in the supernatant using the LL171 (Uzé et al., 1994) reporter cell line.

Co-culture experiments

Bone marrow-derived dendritic cells (BMDCs) were generated as described (Inaba et al., 1992). Briefly, bone marrow cells were cultured in RPMI 1640 medium containing 10% supernatant from X63-mGM-CSF cells for 7-9 days. At least 85% of the resulting cells expressed CD11c and MHC class II as determined by flow cytometry (not shown). Hundred-fifty-thousand tumor cells and 0.5x10^{6} BMDCs were co-cultured in a well of a 24-well plate. After 24h, supernatant was collected and type I IFNs were quantified using the reporter cell line LL171. Alternatively, IFNβ was quantified by ELISA.

In vivo tumor experiments and treatments

Tumor cells were suspended at 2x10^{6}/ml in a 2:1 mix of PBS:Matrigel. Hundred μl of this suspension were injected subcutaneously (s.c.) into the right flank of mice. Tumor size was measured in two dimensions (length and width) every 2-4 days starting on day 7 using a caliper. Immediately before start of interventions, mice were assigned to different experimental groups in such way that the average

and variance of tumor size was similar for each group. Radiotherapy was applied locally on the tumor as a single dose of 1 × 20 Gy with 1.6 Gy/min on day 13 (Surace et al., 2015). Cisplatin (Sandoz) was injected i.p. at 3 mg/kg on day 8 and 13. Control mice were injected with 150 μL of 0.9% NaCl. For immune checkpoint inhibition, anti-PD1 (RMP1-14) and anti-CTLA4 (9H10) monoclonal antibodies were injected i.p. at 250 μg per dose on day 7 and 12. Control mice were injected with 200 μL PBS. $CD8^+$ T cells were depleted on day 9 by i.p. injection of 250 μg of a CD8-depleting antibody (YTS169.4). Control mice were injected with 100 μL PBS. For survival studies, mice were euthanized when the tumor reached a size of 225 mm^2.

Flow cytometry

Excised tumors were collected in RPMI supplemented with 10% FCS and cut into small pieces. Tumor pieces were digested with 1 mg/ml collagenase IV (Bioconcept) at 37°C on a rotating device. After 45 min, 2.6 μg/ml DNaseI (ThermoFisher Scientific) was added and digestion continued for additional 15 min at 37°C. Cells were washed with 0.01 M EDTA in PBS by centrifugation at 350 *g* for 5 min. Red blood cells were lysed using RBC lysis buffer (17 mM Tris pH 7.2, 144 mM NH_4Cl) for 2 min. Cells were washed with PBS and filtered through a 70 μm filter to remove debris. Single cells were stained according to standard protocols. Briefly, cells were surface-stained in 50 μL antibody-mix in PBS. Dead cells were excluded using fixable viability stain according to the manufacturer's instructions. For intracellular cytokine staining, cells were stimulated with 50 ng/ml phorbol 12-myristate 13-acetate (PMA) plus 500 ng/ml ionomycin or with AH-1 peptide (Huang et al., 1996) (SPSYVYHQF, the H-$2L^d$-restricted epitope derived from endogenous retroviral gp70, which is expressed in CT26, 10^{-6} M) for 1 h at 37°C. Subsequently, brefeldin A (10 μg/ml) was added and cells were incubated for additional 3 h. Cells were stained for surface molecules as described above, washed with PBS, and fixed for 30 min on ice using IC Fixation Buffer from Foxp3/Transcription Factor Staining Buffer Set. Subsequently, cells were stained for intracellular IFNγ in 1X permeabilization buffer from the Foxp3/Transcription Factor Staining Buffer Set overnight at 4°C. After washing with 1X permeabilization buffer, samples were suspended in FACS buffer (PBS, 20 mM EDTA pH 8.0, 2% FCS) and acquired using a CyAn ADP9 flow cytometer (Beckman Coulter) or FACS LSRII Fortessa (BD Biosciences).

Due to lack of suitable antibodies for intracellular staining of type I IFN, we detected *Ifnb1* transcripts in single cells by flow cytometry using the PrimeFlow RNA Assay according to manufacturer's protocol. Briefly, single-cell suspensions were surface-stained as described above. Fixation and permeabilization was performed according to manufacturer's instructions. For mRNA detection, *in situ* hybridization with type I Alexa Fluor 568-labeled *Ifnb1* probe was performed for 2 h at 40°C. The signal was amplified by incubating samples for 2 h in PreAmplification reagent at 40°C and additional 2 h at 40°C in Amplification reagent. Samples were incubated with label probes at 40°C for 1 h, washed and acquired on a FACS LSRII Fortessa (BD Biosciences).

For quantitative analysis, CountBright absolute counting beads were used (ThermoFisher Scientific). In all staining, dead cells were excluded using Live/Dead fixable staining reagents (Invitrogen), and doublets were excluded by FSC-A versus FSC-H gating. Samples were analyzed using FlowJo v10 software (Tree Star Inc.). Analysis was performed on single, live cells.

Western blotting

To extract proteins, cells were suspended in RIPA buffer (ThermoFisher) supplemented with protease inhibitor (cOmplete, Mini Protease Inhibitor Cocktail, Roche) and subjected to two freeze-thaw cycles. The protein concentration was determined using the DC Protein Assay (Bio-Rad). For quantification of cGAS and Connexin 43 (CX43, GJA1), a total of 20 μg protein was loaded and for the determination of STING, 100 μg were loaded per lane of a 10% SDS-PAGE gel. Proteins were transferred onto a nitrocellulose membrane (GE Healthcare Life science) with 350 mA for 2 h at 4°C. The membrane was blocked in 5% non-fat milk powder in Tris-buffered saline containing 0.05% Tween-20 (TBS-T) for 1 h at room temperature (RT) or overnight at 4°C. Membranes were stained with the primary antibodies against cGAS (1:1'000), STING (1:1'000), CX43 (1:1'000), α-TUBULIN (1:5'000) or β-ACTIN (1:5'000). Membranes were incubated for 1 h at RT or overnight at 4°C with antibodies diluted in 5% non-fat milk powder in TBS-T. Membranes were washed three times for 10 min in TBS-T and incubated in with the secondary antibody: HRP-goat-anti-mouse IgG (1:10'000) or HRP-goat-anti-rabbit IgG (1:10'000) in 5% non-fat milk powder in TBS-T for 1 h at RT. Membranes were washed three times for 10 min in TBS-T and chemiluminescent reaction was started using the WesternBright ECL kit (Advansta). Protein bands were detected using a Fusion Solo S imager (Vilber). The Precision Plus Protein Dual Color Standard (Bio-Rad) was used to assess molecular weight of protein bands. Relative quantification of cGAS/β-ACTIN and STING/α-TUBULIN ratio was performed using ImageJ software.

Quantification of type I IFN

Type I IFNs were quantified using the reporter cell line LL171. Briefly, $3.5x10^4$ LL171 cells were seeded per well in 96-well flat-bottom plates and incubated with samples for 24 h at 37°C in a CO_2-incubator. Reporter cells were lysed using the Luciferase Cell Culture Lysis 5X Reagent and transferred to a white 96-well LUMITRAC plate (Greiner Bio-One GmbH). Luciferase activity was measured using the Luciferase Assay System in a TECAN plate reader (Tecan). Standard curves were prepared using serial dilutions of recombinant murine IFNβ ranging from 0 to 1'000 pg/ml.

Quantification of cytoplasmic DNA

Tumor cells were seeded at $1x10^6$ cells/well in a 6-well plate and exposed to DNA-damaging treatments. Specifically, cells were irradiated with 8 or 20 Gy using a RS2000 (Radsource) irradiation machine at 6.7 Gy/min or treated with 15 μM Cisplatin (Sandoz).

Cytoplasmic dsDNA was measured in live cells 24 h later. As a control, 1x10^6 fresh splenocytes were used. The cytoplasmic fraction was extracted using the NE-PER Nuclear and Cytoplasmic Extraction Reagents. Cytoplasmic dsDNA was quantified using the AccuClear Nano dsDNA Assay Kit and a SpectraMax i3 (Molecular Devices) microplate reader as described (Vanpouille-Box et al., 2017).

Quantification of cytokines in tumor lysates

Pieces of excised tumors were snap-frozen in liquid nitrogen and stored at −80°C. To prepare a lysate, 2x weight in volume of PBS supplemented with protease inhibitor was added to frozen tumor pieces. Zirconium oxide beads were added, and samples were homogenized for 30 s at 5 m^2/s^2 using a FastPrep® instrument using. Samples were centrifuged at 4°C at 14'000 *g* for 15 min. The supernatant was collected on ice and immediately used. Total protein concentration was measured using DC Protein Assay (Bio-Rad). Cytokines were quantified in lysates using the LEGENDplex Mouse Inflammation Panel according to manufacturer's instructions. Samples were acquired on CyAn ADP9 flow cytometer (Beckman Coulter). IFNβ was quantified by ELISA and read on a SpectraMax i3 (Molecular Devices) plate reader.

Four-color immunofluorescence

For antigen-retrieval, slides were heated for 2 h at 55°C and incubated in Trilogy pretreatment solution (CellMarque) in a pressure cooker for 15 min. After cooling for 15 min, slides were washed with milli-Q to remove remaining paraffin and treated with 3% H_2O_2 in H_2O for 15 min. Slides were washed with milli-Q water and incubated with 4% BSA/0.01% Triton X-100 in PBS for 15 min at 37°C to prevent unspecific binding of antibodies. Subsequently, slides were incubated overnight at 4°C or 3 h at RT with a primary antibody diluted in 1% BSA/0.01% Triton X-100 in PBS. Following primary antibodies were used: anti-cGAS (1:500), anti-Pan-Cytokeratin (1:2000) and anti-CD8 (1:1000). After incubation, slides were washed 3 times for 5 min with 0.01% Triton X-100 in PBS and incubated for 1 h at RT with following HRP-conjugated secondary antibodies: Donkey-anti-rabbit IgG (1:1'000) and donkey-anti-mouse IgG (1:1'000), diluted in 1% BSA in 0.01% Triton X-100 in PBS. The signal was amplified using 1:100-diluted fluorophore-conjugated tyramides Opal 520, Opal 540 and Opal 690 in amplification buffer (PerkinElmer) for 10 min at RT. Slides were washed subsequently and boiled for 12 min in 10 mM citric acid pH 6.0 to strip the bound antibodies. Blocking and incubation with the next primary and secondary antibody, tyramide amplification and stripping was repeated for different targets that were consecutively detected. Finally, slides were washed, incubated with 0.5 μg/ml 4′,6 diamidine-2-phenylindole (DAPI; Invitrogen) for 5 min, washed again and mounted with ProlongDiamond medium (Invitrogen).

Calcein AM transfer assay

Tumor cells were washed twice with PBS and labeled with Calcein AM dye (5 μg/ml in PBS) at 37°C for 30 min in the dark. Cells were washed twice with PBS and 0.5x10^6 cells were plated in complete RPMI in a well of a 12-well plate. Five-hundred-thousand BMDCs were added to the tumor cells and incubated at 37°C for 6 h. Cells were collected, washed with PBS and surface-stained with fluorescently-labeled antibodies. After washing with PBS, samples were acquired using a CyAn ADP9 flow cytometer (Beckman Coulter). Calcein AM was detected in the FITC-channel.

Quantification of gamma-H2AX

Four-chambered culture slides (BD Falcon) were treated with poly-L-lysine for 10 min and dried for 2 h at RT. Seventy-five thousand $CT26^{ctrl}$ and $CT26^{\Delta Mb21d1}$ were grown per chamber overnight. Cells were left untreated, irradiated with 1 Gy or 5 Gy and incubated for 1 h. Slides were briefly washed with PBS and incubated with the pre-extraction solution (25 mM HEPES pH 7.7, 50 mM NaCl, 1 mM EDTA, 3 mM $MgCl_2$, 300 mM sucrose, 0.5% Triton X-100) for 5 min on ice. After washing with PBS, cells were fixed with 4% paraformaldehyde in PBS for 15 min at RT. To prevent unspecific binding of antibodies, slides were incubated with 1% BSA in PBS for 15 min. Slides were incubated with anti-gamma-H2AX (1:200, Millipore) in 1% BSA in PBS for 90 min at RT. Slides were washed and incubated with the AlexaFluor568-coupled secondary antibody goat anti-mouse IgG (1:400, Life Technologies) in 1% BSA in PBS in the dark for 30 min at RT. Slides were washed three times with PBS and stained with 0.5 μg/ml 4′,6 diamidine-2-phenylindole (DAPI; Invitrogen) in deionized H_2O for 5 min, washed again and mounted with FluoroMount medium (Invitrogen). Immunofluorescent images were captured on a DM6 B fluorescent microscope (Leica Biosystems) using an oil-immersion objective (63x/1.4 NA). The automated image acquisition was performed on an IX83 microscope (Olympus) equipped with ScanR imaging platform and 40x/0.9 NA objective. Nuclei were identified based on DAPI signal, and the intensity of gamma-H2AX for each nuclear object were analyzed using the Analysis ScanR software. At least 500 nuclei were analyzed per sample.

Colony-forming assay

The colony-forming assay was performed according to the description in Franken et al. (2006). Briefly, 10, 50 and 100 $CT26^{ctrl}$ and $CT26^{\Delta Mb21d1}$ were seeded in one well of a 6-well plate in duplicates and incubated for 4 h at 37°C. Cells were left untreated, irradiated with 2, 4, 5, 6 or 9 Gy or treated with Cisplatin (Sandoz) at concentrations of 1, 3, 15 or 30 μM. Cells were incubated for 6 days to form colonies. Colonies were washed with PBS, fixed and stained with 6% glutaraldehyde, 0.5% crystal violet in H_20 for 30 min. Fixation-staining solution was removed and wells were rinsed several times carefully with tap water. Plates were dried at RT and colonies

counted by eye. For the untreated control, the plating efficiency was calculated as followed: [# colonies ÷ # cells seeded] x 100%. For each treatment condition, the surviving fraction was calculated as follows: # colonies ÷ [# cells seeded x plating efficiency].

QUANTIFICATION AND STATISTICAL ANALYSIS

Quantification of immunofluorescence data

Stained slides were scanned using the automated multispectral microscopy system Vectra 3.0 (PerkinElmer). Six to 8 representative areas of tumor tissue were imaged at 200-fold magnification. Inform software (PerkinElmer) was used for spectral unmixing of individual fluorophores and autofluorescence, and to apply cell segmentation and quantification algorithm on the slide as described (Siliņa et al., 2018a, 2018b). Samples were excluded where the area was damaged, or the algorithm was not identifying properly.

Statistical analysis

Group sizes, number of replications, and explanation of the mean and error bars are provided in the figure legends. Statistical tests were performed with GraphPad Prism 7.0 (GraphPad Software). For comparison of two experimental groups, the unpaired two-tailed Student's t test was used, unless stated otherwise. When more than two groups were compared, the one-way ANOVA with Tukey's multiple comparison correction was used. Survival data were analyzed with a Log-rank (Mantel-Cox) test. *$p < 0.05$, **$p < 0.01$, ***$p < 0.005$, ****$p < 0.001$. Data are shown as mean ± SD unless specified otherwise.

DATA AND CODE AVAILABILITY

This study did not generate any unique datasets or code.